This is a peer-reviewed, author's accepted manuscript of the following research article: Patel, D., Perez-Sanchez, G., Jorge, M., Ray, D., Aswal, V. K., Kuperkar, K., Coutinho, J. A. P., & Bahadur, P. (Accepted/In press). Rationalising design of pluronics-surfactant mixed micelles through molecular simulations and experiments. *Langmuir*.

# Rationalising design of Pluronics-surfactant mixed micelles through molecular simulations and experiments

Divya Patel[a], Germán Pérez-Sánchez[b], Miguel Jorge[c], Debes Ray[d,e], Vinod K. Aswal[d], Ketan Kuperkar[a,*], João A. P. Coutinho[b], Pratap Bahadur[f]

[a] *Department of Chemistry, Sardar Vallabhbhai National Institute of Technology (SVNIT), Ichchhanath, Surat-395 007, Gujarat, INDIA.*
[b]*CICECO – Aveiro Institute of Materials, Department of Chemistry, University of Aveiro, Aveiro, 3810-1933, PORTUGAL.*
[c]*Department of Chemical and Process Engineering, University of Strathclyde, 75 Montrose Street, Glassgow G1 1XJ, UNITED KINGDOM.*
[d]*Solid State Physics Division, Bhabha Atomic Research Centre (BARC), Trombay, Mumbai, 400 085, Maharashtra, INDIA.*
[e]*Biomacromolecular systems and processes, Institute of Biological Information Processing, Forschungszentrum Julich- 52428, GERMANY.*
[f]*Department of Chemistry, Veer Narmad South Gujarat University (VNSGU), Udhana-Magdalla road, Surat-395 007, Gujarat, INDIA.*

***Corresponding author:** E-mail: ketankuperkar@gmail.com

**Declaration of interest:** None

**ABSTRACT**

Aqueous systems comprising polymers and surfactants are technologically important complex fluids with tuneable features dependant on the chemical nature of each constituent, overall composition in mixed systems and solution conditions. The phase behavior and self-assembly of amphiphilic polymers can be changed drastically in the presence of conventional ionic surfactants and needs to be clearly understood. The phase behavior and self-aggregation dynamics of a triblock copolymer (Pluronics® L81, $EO_3PO_{43}EO_3$) in the presence of three cationic surfactants (with 12C long alkyl chain but with different structural features) viz. dodecyltrimethylammonium bromide (DTAB), didodecyldimethylammonium bromide (DDAB), and ethanediyl-1,2-bis(dimethyldodecylammonium bromide) (12-2-12) were investigated in aqueous solution environment. The nanoscale micellar size expressed as hydrodynamic diameter ($D_h$) of copolymer-surfactant mixed aggregates was evaluated using dynamic light scattering (DLS) while the presence of varied micellar geometry of L81-cationic surfactant mixed micelles were probed using small-angle neutron scattering (SANS) approach. The obtained findings were further validated from molecular dynamics (MD) simulations, employing a simple and transferable coarse-grained (CG) molecular model based on the MARTINI force field. L81 remained molecularly dissolved upto ~20 ºC but phase separates forming turbid/ translucent dispersion close to its CP and existed as unstable vesicles. However, it exhibited interesting phase behavior expressed in terms of blue point (BP) and *double* cloud point (CP) with the progressive addition of different cationic surfactants leading to mixed micellar systems with triggered morphology transition from unstable vesicles to polymer-rich micelles to cationic surfactant-rich micelles. The energetics of the clouding phenomenon assessed for the copolymer in the presence of cationic surfactants showed a stamped expansion in CP which is attributed to the non-cooperative association of L81 and surfactants. Such amendment in the morphology of copolymer nanoaggregates in the presence of cationic surfactants has been well ascribed from scattering data. This is further rationalized employing the molecular dynamics (MD) approach which validated the effective interactions between Pluronics®-cationic surfactant mix micelles. Thus, our experimental results integrated with MD yield a deep insight on the nanoscale interactions controlling the micellar aggregation (Pluronics®-rich micelles and surfactant-rich micelles) in the investigated mixed system.

***Keywords:*** Pluronics®; cationic surfactants; mixed micelle; scattering, molecular dynamics simulation

## GRAPHICAL ABSTRACT

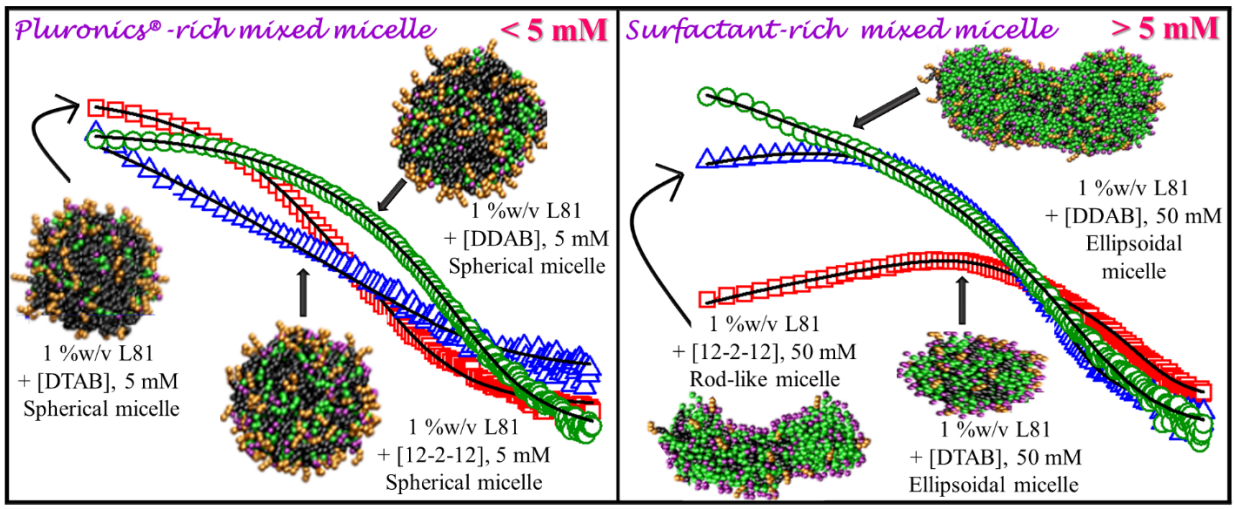


*Scattering profiles and representation of the L81 Pluronics®-rich and ionic surfactant-rich mixed micelles obtained by CG-MD simulations.*

## INTRODUCTION

Surfactants are extensively used in scientific, technical and industrial applications due to their superior adsorption and micellization properties in aqueous solution environment and so have received considerable attention for several decades. In particular, poly(ethylene oxide, EO)-poly(propylene oxide PO)-poly(ethylene oxide, EO)-based triblock copolymers, known as Pluronics®, constitute a class of commercially available non-ionic surfactants offering a wide hydrophile-lipophile balance (HLB) range that have found interest in the biomedical field as quality conveyance vehicles, sensitizers, and part of pharmaceutical formulations, besides being used in personal care products, textiles, inks, coatings, among others.[1-4] The Pluronics® are highly surface-active macromolecules that undergo self-assembly thereby forming nanoscale aggregates (micelles) above the critical micelle concentration (CMC) or critical micelle temperature (CMT), whose hydrophobic core is shaped by solvated PPO blocks and encompassed by an external shell of completely hydrated PEO end chains.[5-8]

Other surfactants are often added to Pluronics® to tune their solution properties and to improve their colloidal stability.[7-11] Mixed Pluronics®-surfactants systems have been examined for understanding their synergistic/antagonistic interactions that give rise to some beneficial properties such as increase in CP, enhanced solubilization of hydrophobic substances, or inducing charge on mixed micelles.[2,7-9] The mixed micellar systems offer better interfacial and colloidal properties in comparison to their individual counterparts, and are often beneficial in practice. Several reports have proved that the cleansing properties of Pluronics® that can be modulated with the addition of other surfactants.[9,12-14] Consequently, the total amount of surfactant necessary for a desired application can be reduced, which leads to a decrease of both the environmental and the economic impacts. Hence, binary aqueous mixtures of non-ionic amphiphilic Pluronics® and ionic surfactants have attracted significant attention in applied research.[1,3,5,8,15] Reported results show that the strong interaction between ionic surfactants and uncharged Pluronics® lead to the formation of charged mixed micelles with decreasing size that finally transforming to very small ionic surfactant-rich micelles at high surfactant concentrations. However, the nature and strength of this synergy rely upon a delicate balance between the charge and hydrophobicity of both the polymer and surfactant.[8,11,15] Prior studies have revealed that amongst all the ionic surfactants, the anionic surfactants displayed the strong synergistic interaction modufying the colloidal behavior of Pluronics® solutions.[8,16-19] Also, the Pluronics® and cationic surfactant blended micellar systems are getting a lot of consideration in the area of surfactant science and technology.[8,20-23] The formation of mixed micelles and their dependence on environmental factors (temperature, pH, additives, etc.), counter-ion

binding, thermodynamic and other parameters, must be investigated to achieve a deep understanding on their physicochemical behavior with implications on their application prospects.

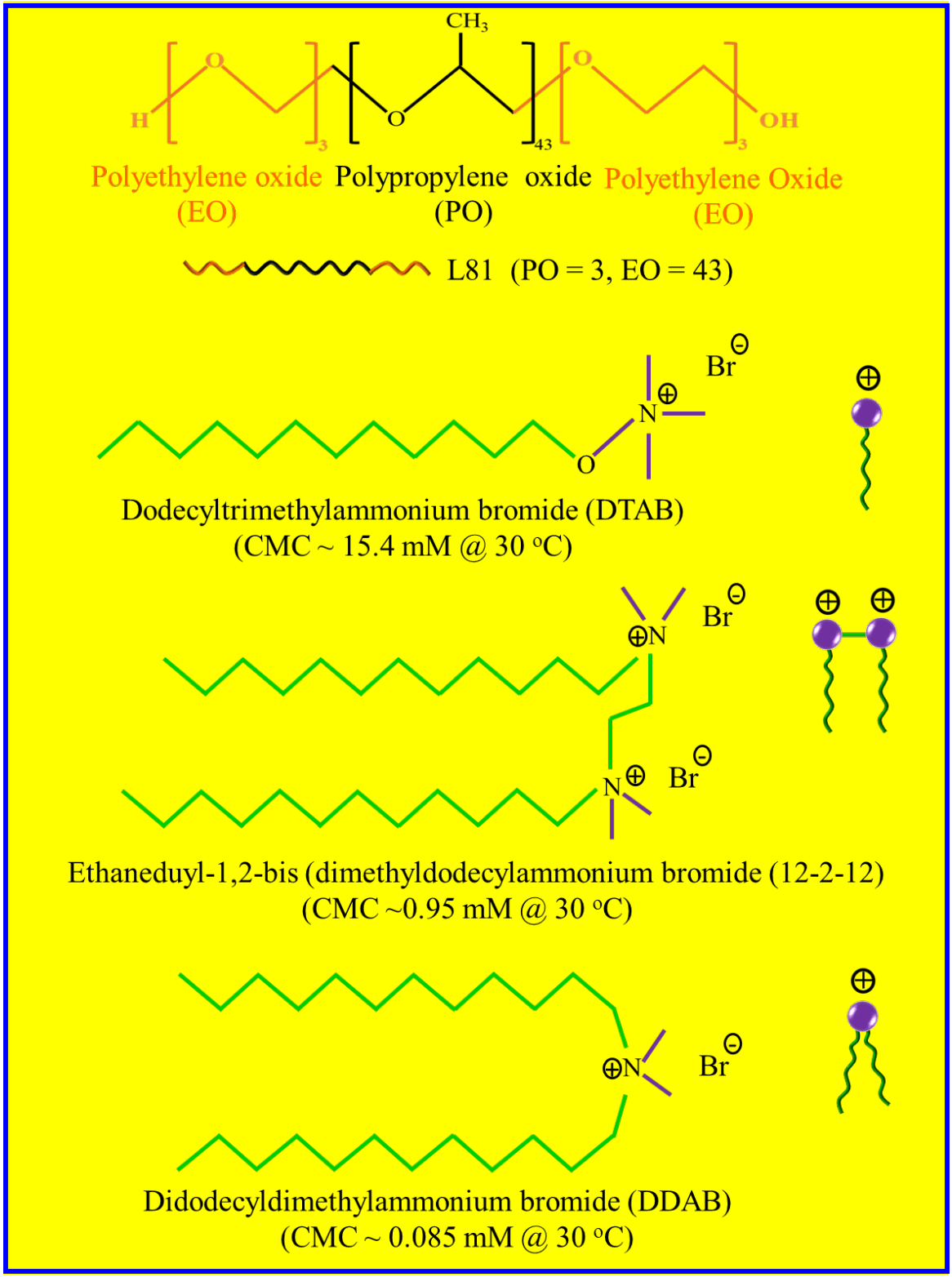


**Scheme 1.** Structure formulae and properties of the surfactants used in this study.

In recent years, computer simulation methods have emerged as a powerful and efficient tool to study the aggregation behavior of surfactants. The molecular dynamics (MD) simulation approach has been extensively used to explore the dynamics and morphology dependence of surfactant architecture in varied frameworks.[24-29] A detailed knowledge of the molecular scale interactions governing the self-assembly is of great importance to design an effective Pluronic®-surfactant mixed system. Thus, the present work reports the self-assembly and aggregation behavior in Pluronic®-cationic surfactant mixed systems employing phase separation study and small-angle neutron scattering (SANS). L81 Pluronic® was chosen because it forms vesicle structures and we are particularly interested in analysing the effect of surfactant on those aggregates. Here, the selected cationic surfactants contain alkyl chains with 12 carbon atoms (12C) with bromide counterion but differ in structure and degree of hydrophobicity i.e., single chain DTAB, double chain DDAB and dimeric (gemini) 12-2-12, as illustrated in **Scheme 1**.

The choice of these cationic surfactants was made based on their different micellization behavior in aqueous solution environment i.e., DTAB forms small spherical micelles (CMC ~ 15.4 mM at 30 ºC)[5], 12-2-12 forms cylindrical/rod-like micelles (CMC ~ 0.95 mM at 30 ºC) [6], while DDAB (CMC ~ 0.085 mM at 30 ºC)[6] remains insoluble in water due to its high Krafft point (< 16 ºC) and forms vesicles/lamellar structures in dilute solution at ambient temperature. In this study, the concentration of Pluronics® L81 solution is taken as 1 %w/v and 3 %w/v while the surfactant concentration ranged from 0-50 mM. The phase behavior of L81 in the presence of cationic surfactants in varying concentration, expressed as cloud point (CP), will be examined and followed by the scattering measurements. MD simulations using a coarse-grained (CG) model were carried out to rationalize our experimental data and provide a platform for screening of potential systems. The employed model is expected to allow to study how the L81 aggregates transform into mixed micelles, and the consequent changes in CP, in the presence of the cationic surfactants with different structural and solution properties.

## METHODOLOGY

### Materials

Pluronics® L81 was received as a gift sample from BASF, NJ, USA. The cationic surfactants: dodecyltrimethylammonium bromide (DTAB, ≥ 98% purity), didodecyl-dimethylammonium bromide (DDAB, 98% purity), and ethanediyl-1,2-bis(dimethyldodecyl-ammonium bromide) (12-2-12, 98% purity), used as additives were purchased from Merck, India. All the compounds were used without any further purification. Solutions were prepared in deuterium oxide ($D_2O$) for neutron scattering experiments to produce a very good contrast between the hydrophobic core and the solvent, while double-distilled water was used for solution preparation for the remaining experiments.

### Experimental Methods

To achieve the study in conditions of Pluronics®-rich micelle or ionic surfactant-rich micelle for our investigated system, we have selected the concentration of Pluronics® as 1 %w/v while varying the concentration of cationic surfactants. However, as this concentration was too low to form a sufficient number of micelles in mixed Pluronic/surfactant simulated systems within a reasonable amount of computational time, we have also employed a 3 %w/v Pluronics® solution in the presence of varying concentrations of cationic surfactants to enable a more direct comparison between simulations and experiments.

### Phase behavior

The phase separation ($2\phi$) phenomenon expressed as cloud point (CP) was scrutinized in Pluronics® L81 to perceive the impact of cationic surfactants (DTAB, DDAB and 12-2-12) in triggering the phase changes due to varied aggregation. Here, the CP has been determined by observing an abrupt turbidity appearance in the solution with progressive temperature increase. The CP measurements were repeated a minimum of three times within a temperature range of ± 0.1 °C.[16,17,30,31]

### Scattering silhouette

The hydrodynamic diameter ($D_h$) of micelles and vesicles were obtained from dynamic light scattering (DLS) for the examined mixed systems employing Zetasizer (Malvern Instruments, UK). The He-Ne, 4 mW laser (wavelength $\lambda_o$ = ~ 635 nm) was used as the incident beam with the scattering angle 90°. The $D_h$ was recorded considering three consecutive measurements for each sample.[16,30-34]

Small-angle neutron scattering (SANS) experiments were performed on the selected 1 %w/v and 3 %w/v Pluronics® L81 solutions to determine the aggregate size and shape using SANS diffractometer at Dhruva reactor, BARC, Mumbai, India. The measured scattering data

were corrected by SASFIT software where coherent differential scattering cross-section ($d\Sigma/d\Omega$) per unit volume was evaluated as a function of wave vector transfer Q ($= 4\pi\sin\theta/2)/\lambda$, where $\lambda$ is the wavelength of the incident neutrons and $\theta$ is the scattering angle).[11,15,30-34]

The models used for SANS data analysis have been described in detail in the Supporting Information.

**Computational Methods**

*Simulation details*

All simulations were performed with the molecular dynamics GROMACS 2019 software package[35] by integrating the equations of motion using the leapfrog algorithm[36] with a 20-fs time step (standard for CG simulations). Bonded interactions, i.e., bond stretching and angle bending, were held rigid with the Linear Constraint Solver (LINCS)[37], whereas non-bonded interactions comprised Lennard-Jones (LJ) and Coulomb functions. Long-range electrostatic interactions were computed using the Particle-Mesh-Ewald (PME) method[38]. The non-bonded interactions were computed with the Verlet cut-off scheme (potential-shift-Verlet modifier) and a cut-off of 1.2 nm. Unless otherwise stated, the temperature was set to 333 K with the velocity-rescaling thermostat[39] using a coupling time constant of 1.0 ps. The Parrinello-Rahman barostat[40] was used to maintain the pressure at 1 bar using an isotropic coupling with a time constant of 24.0 ps. The simulation boxes were created with Packmol[41] with all molecules distributed randomly, and NpT ensemble production runs were performed with periodic boundary conditions in all directions. Previously, an energy minimisation step was performed for the initial simulation boxes using the steepest descent algorithm to avoid close contacts between molecules. Afterwards, two equilibration MD simulations were carried out in the NVT and NpT ensembles to set the proper temperature and density, respectively. The total potential energy, pressure, temperature, and density were monitored along the equilibration and production stages to ensure that thermodynamic equilibrium was reached. The Visual Molecular Dynamics (VMD) software package[42] was used to visualise the MD trajectories. The formation of aggregates was analysed using an in-house code[43] based on the Hoshen–Kopelman cluster-counting algorithm[44].

*Coarse-grained molecular model*

The CG model based on Martini v2.2[45] for diluted Pluronic® aqueous solutions[18] was selected for the L81 Pluronic®, whereas the models for DTAB, DDAB and 12-2-12 surfactants were taken from Wang et al.[17]. It must be noted that some minor changes were implemented, as explained below. For DTAB, we have considered only one $C_2$ bead acting as a linker

between the charged head groups and the alkyl tail, thus adopting a 4:1 mapping rather than the 3:1 mapping used by Wang et al. In this regard, the DTAB CG model is closer to the accepted CG Martini-based mapping that was successfully used in many studies[46-49]. For 12-2-12, the CG model for 16-2-16[17] was taken where one $C_2$ bead was removed from each alkyl tail. Similarly, the DDAB model was constructed based on the above 12-2-12 model but removing one of the charged $Q_0$ beads. **Figure 1** summarises the CG mapping used in this work for all compounds, where the L81 CG model consists of $SP_1$ and $SC_3$ beads (representing mildly polar and non-polar beads, respectively, both with 3:1 mapping) to describe the PEO and PPO segments, respectively. The CG model for the cationic surfactants includes $Q_0$ (representing ionic beads with no hydrogen bond donor/acceptor character) for charged head groups. The alkyl-chains were mapped with non-polar $C_2$ beads for those methyl groups acting as a bridge between the charged head group and the alkyl-chain, whereas $C_1$ beads were selected for the remainder of the alkyl tails. The $Q_a$ (ionic hydrogen bond acceptor) bead was selected for $Br^-$ counterions, which implicitly includes the effect of 6 solvating water molecules, mimicking the first hydration shell. The regular Martini v2.2 water model was chosen where $P_4$ beads implicitly include four water molecules. 10% of antifreeze "big" $BP_4$ water beads were added to disturb the lattice packing of equally sized beads since the σ value of the Lennard-Jones potential in $BP_4$-$P_4$ interactions is scaled to 0.57 nm rather than the 0.47 nm in $P_4$-$P_4$ interactions, thus preventing artificial freezing of the water phase[45].

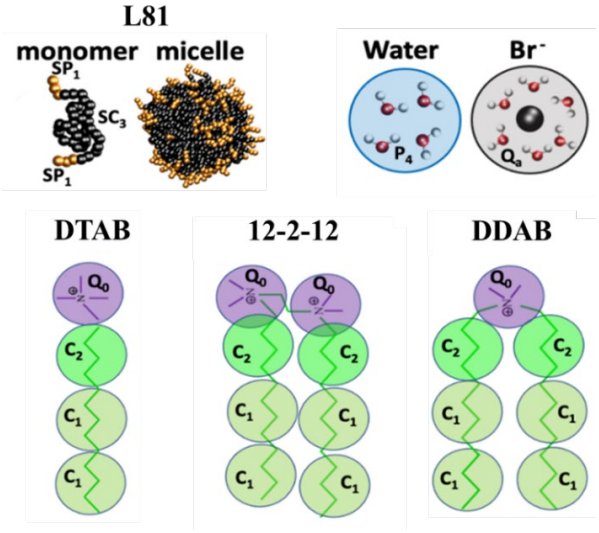


**Figure 1**. CG mapping for the L81 Pluronic, DTAB, DDAB and 12-2-2 cationic surfactants. The black and orange colours in the L81 Pluronic represent the PPO and PEO segments, respectively. Purple colour was chosen for charged headgroups ($Q_0$), light green for a polar beads ($C_2$) linking the above headgroups with the alkyl tails whereas dark green beads ($C_1$) represent the alkyl tail end. The $P_4$ regular water Martini v2.2 model was chosen (blue) while hydrated bromide counterions were described by a $Q_a$ bead (grey).

Since some changes from the original Wang et al.[17] CG model were implemented, a validation test was carried out to ensure that the CG model can reproduce the experimental micelle distributions. Thus, a set of four CG-MD simulation tests for the individual compounds (L81, DTAB, DDAB and 12-2-12) in aqueous solution were performed for 3000 ns of simulation time to ensure that the correct thermodynamic equilibrium is reached. First, a 1 %w/v L81 concentration (run1) was equilibrated in a 30 nm side simulation box. The simulation runs carried out in this work are summarised in Table S1 of Supplementary information.

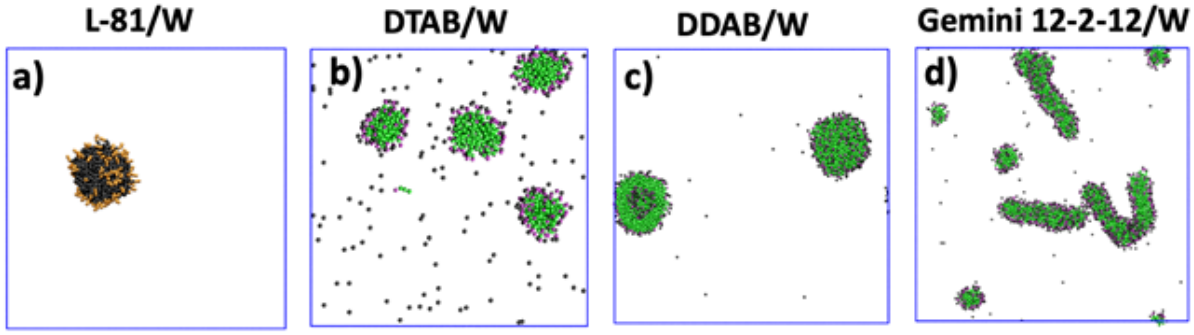


**Figure 2**. CG-MD simulations snapshots after 3000 ns of simulation time for aqueous solutions of L81 (a), DTAB (b), DDAB (c) and 12-2-12 (d) at 1 %w/v of concentration and a temperature of 298 K, except for the 12-2-12 system which was run at 303 K to compare with available experimental data. Water molecules were removed for clarity. The colour code is the same as in **Figure 1** with bromide counterions in black for the cationic surfactant systems.

**Figure 2a** shows the final simulation snapshot where all L81 molecules quickly self-assemble into a single large aggregate, reflecting the fact that L81 is highly hydrophobic. This system was run with only 50 L81 because simulating Pluronics® at this level of molecular weight and under dilute conditions is highly computationally demanding. Experimental results suggest that no micelles are found even under dilute conditions but relatively large aggregates are formed instead, exhibiting sizes around 200 nm and aggregation numbers of $N_{agg}$> 300[47-51]. Our simulations are consistent with this behavior. **Figure 2b** shows the spherical micelles obtained in the 1 %w/v DTAB aqueous solution (run2) with average $N_{agg}$ = 60 and Ø = 3.4 nm, in good agreement with experimental results found in the literature[52,53]. **Figure 2c** confirms the formation of vesicles in the DDAB aqueous solution (run3) as demonstrated by many experiments[54-57]. In fact, after 3000 ns of simulation, the DDAB formed two vesicles with average $N_{agg}$ ~ 250 and a size Ø ~ 7 nm, in good agreement with the light scattering measurements reported by Marques et al.[58]. Finally, **Figure 2d** shows the formation of poly-dispersed aggregates in the 12-2-12 aqueous solution (run4), revealing an aggregate size distribution in the range of $N_{agg}$ ~ 50/100, besides exhibiting some elongated micelles, as also

observed in previous computational[59] and experimental studies[10,60,61,62]. These validation tests give us confidence that the CG model is realistically describing the self-assembly behavior of all the individual components of the system, and hence can be used to infer mechanistic information and make predictions about the behavior of more complex mixtures.

## RESULTS AND DISCUSSION

### Phase behavior

The CP (which is often related to the dehydration of the PEO moiety with the progressive increase in temperature) of 1 %w/v L81 i.e., ~ 20 °C along with their CMT (< 20 °C) are in accordance with the literature data[16,30]. The degree of hydrophobicity exhibited by the three cationic surfactants followed the order: DTAB < 12-2-12 < DDAB[5,6,63,64]. Studies have also inferred that the clouding phenomenon in this conventional Pluronics® can be impacted by the presence of additives, where both deferral and improvement were noticed[28,31,65-67]. A small amount of ionic surfactant drastically influences the CP of Pluronics®. The temperature-dependent solution behavior for the examined Pluronics®-cationic surfactants blended systems is presented in **Figure 3**. This clouding behavior compelled us to attempt understanding the phase behavior of L81 (1 %w/v and 3 %w/v) in aqueous solution.

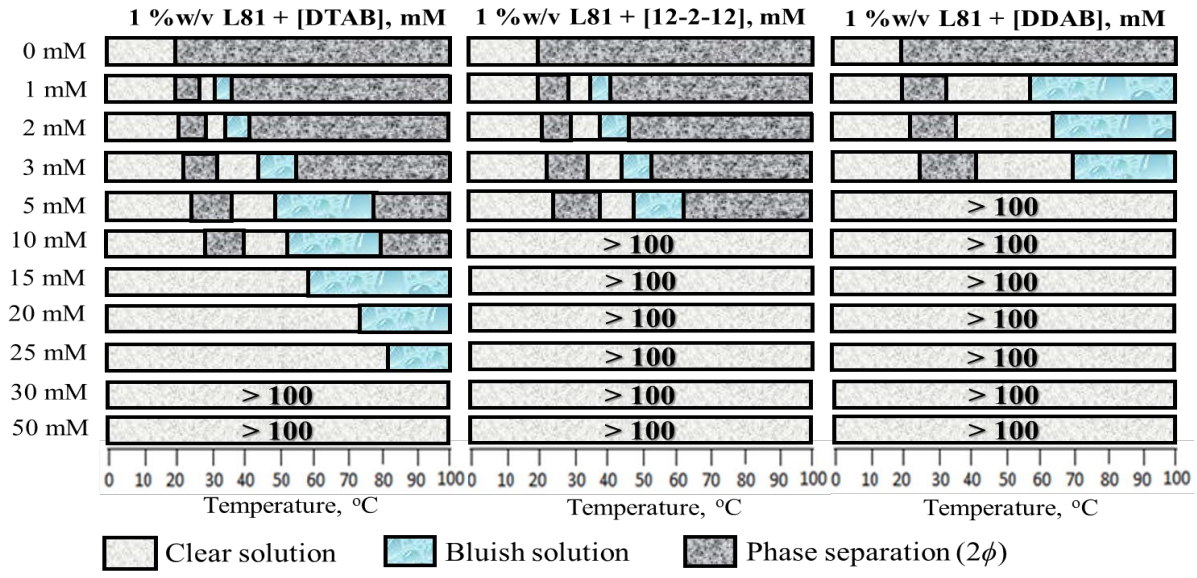


**Figure 3a.** Representation of the temperature dependent behavior of in 1 %w/v L81 solutions in presence of varying concentration of cationic surfactants (left axis).

The addition of the cationic surfactants in varying concentrations (0-50 mM) to 1 %w/v Pluronics® solution leads to a physical demarcation in the solution *i.e.*, *single* (first) CP when subjected to increasing temperature. However, some mixed Pluronics®-cationic surfactant systems even displayed a *double* CP, which could be due to the growth of micelles at the

temperature (as revealed by the bluish region) close to their *double* CP as depicted in **Figure 3a.**

For 1 %w/v L81 in the presence of 1 mM-10 mM DTAB i.e., before its CMC (*pre-micellar region*), the system shows *double* CP. The first CP observed is solely due to L81 undergoing phase separation. This suggests the presence of Pluronic®-rich micelles with negligible influence of DTAB on the L81 behavior. A persistent increase in the temperature induces the Pluronic®-rich micellar assembly to solubilize more DTAB forming first a colourless and then a bluish solution, progressively leading to 2$\phi$ (*double* CP). However, 1 %w/v L81 in the presence of 15 mM-25 mM DTAB i.e., at and above CMC (*post-micellar region*), the system does not show any evidence of CP; only the bluish region is observed. This suggests that the presence of 15 mM-25 mM DTAB contributes to the formation of mixed micelles. With further increasing the DTAB concentration above 30 mM, no 2$\phi$ is observed i.e., CP > 100 $^{o}$C which may be due to the presence of high concentration of cationic surfactant, thereby forming cationic surfactant-rich mixed micelles.

A similar trend is followed in 1 %w/v L81 for [12-2-12] and [DDAB], albeit at different concentration ranges. The CP appears between 1 mM to 5 mM for 12-2-12 and between 1 mM to 3 mM for DDAB, while above those respective concentrations, no 2$\phi$ is observed i.e., CP is above 100 $^{o}$C. However, while the solutions with a low concentration of 12-2-12 show *double* CP, the corresponding DDAB solutions show only one CP which on further heating appears bluish with no evidence of CP. The behavior of the DDAB solution is most likely due to its very low CMC and enhanced hydrophobicity. As observed for DTAB, increasing concentration of 12-2-12 and DDAB with 1 %w/v L81 leads to the formation of surfactant-rich mixed micelles.

Likewise, the phase behavior was observed for 3 %w/v L81 with cationic surfactants (0 mM – 90 mM) (**Figure 3b**) which followed a similar trend as observed in the case of 1 % w/v L81 solutions. Here, at low temperature and lower concentration (5 mM to 10 mM) of cationic surfactants (DTAB and 12-2-12), the additives do not get solubilized in L81 micelles so that the system displays 2$\phi$ close to CP of L81 (1$^{st}$ CP). After this, it was observed that the cationic surfactants were found to solubilize in L81 micelles forming a clear solution. On progressive heating, the solution turns bluish indicating the presence of some bigger micellar assembly which finally leads to 2$\phi$. As such, although the transition points change with concentration of L81, the qualitative behavior is the same in both systems.

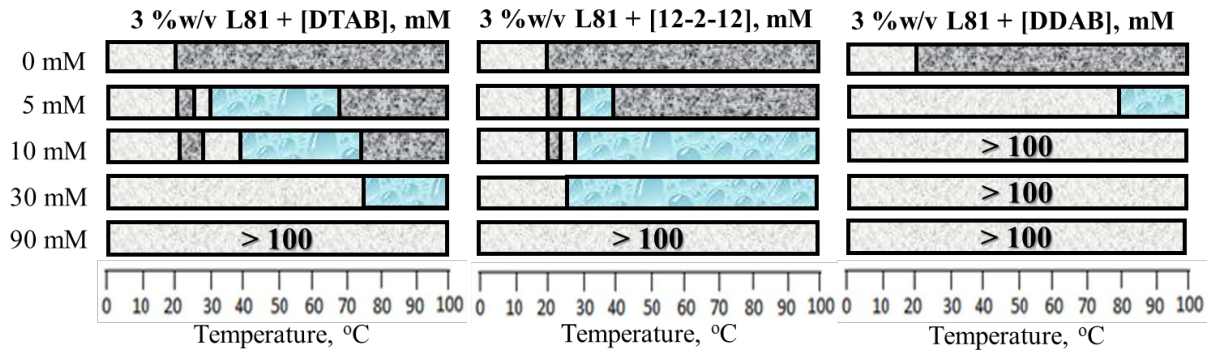


**Figure 3b.** Clouding behavior in 3 %w/v L81 with cationic surfactants at various concentrations (left axis).

The scattering data outlined in **Figures 4** and **5** illustrate the critical relationship between the Pluronics®-cationic surfactant mixed systems, demonstrating the important role of hydrophobic interactions expressed in terms of hydrodynamic diameter ($D_h$), which sheds light on the solubilization of cationic surfactants in L81 micelles.

It was clearly observed that the 1 %w/v L81 solution showed $D_h$ ~114.8 nm at 30 °C, which firstly increases with addition of 1 mM DTAB (~ 140.6 nm) likely due to the incorporation of cationic surfactant molecules into polymer-rich mixed micelles. On increasing the concentration of DTAB from 3 mM to 50 mM, the system shows a drastic fall in $D_h$ i.e., it appears as ~ 41.0 nm (3 mM), ~ 19.1 nm (10 mM), ~ 8.9 nm (30 mM), and ~ 6.5 nm (50 mM) at 30 °C. This is most likely due to a transition from large polymer-rich to the much smaller cationic surfactant-rich micelles as the cationic surfactant concentration increases **(Figure 4a)**. A similar trend was followed with 12-2-12. Here, too, the $D_h$ increases initially in the presence of 1 mM 12-2-12 (~ 166.56 nm). However, increasing the concentration of 12-2-12 from 3 mM to 50 mM, the $D_h$ falls drastically i.e., ~ 62.63 nm (3 mM), ~ 25.3 nm (10 mM), ~ 10.3 nm (30 mM), and ~ 7.2 nm (50 mM), at 30 °C **(Figure 4a)**. Unlike DTAB and 12-2-12, no such significant change in $D_h$ was noticed in the case of DDAB, which again could be due to its more hydrophobic nature **(Figure 4a)**.

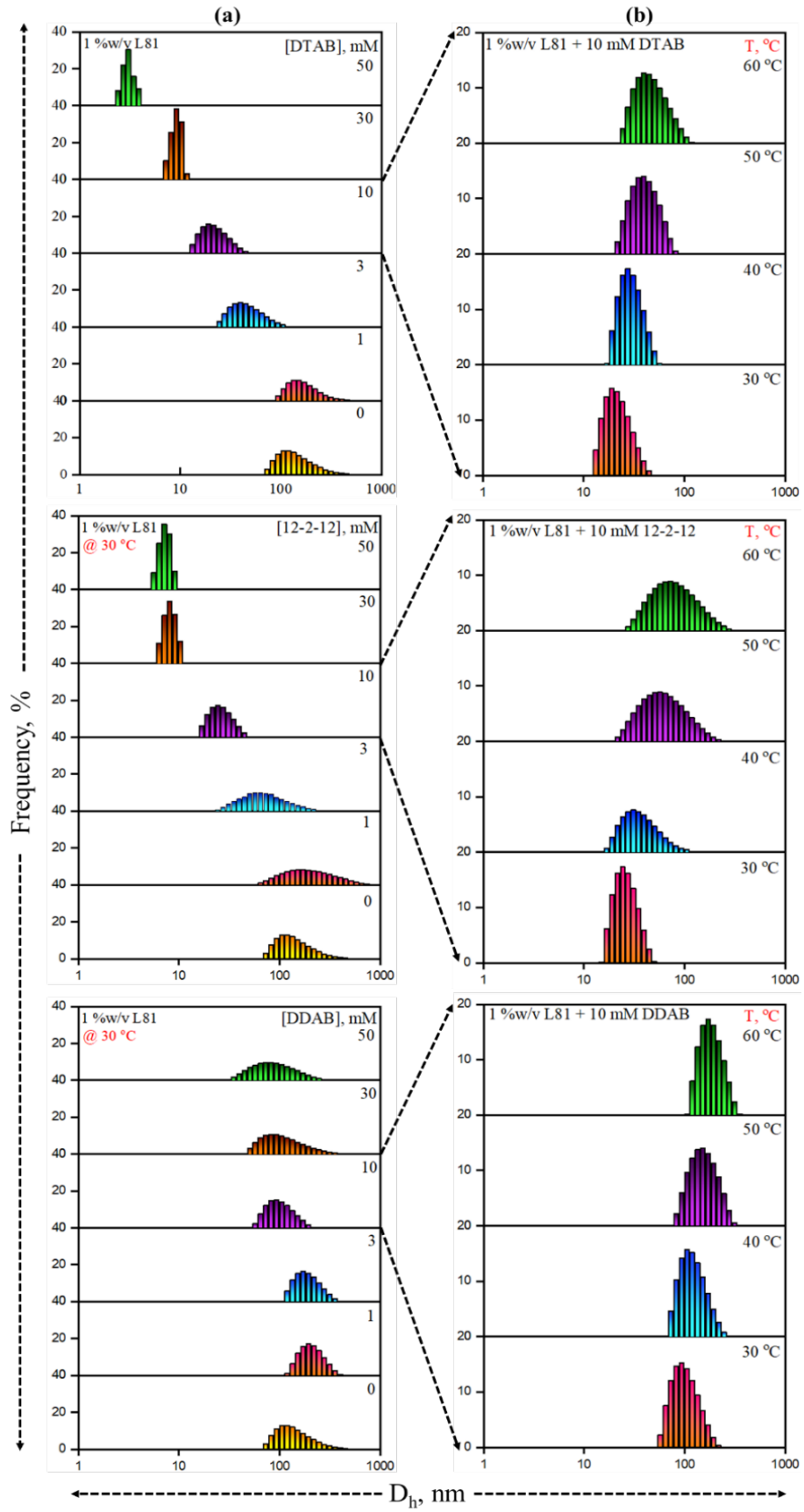


**Figure 4.** Size distribution profiles expressed in frequency versus hydrodynamic diameter ($D_h$) for (a) 1 %w/v L81 with increasing concentration of different cationic surfactants at 30 °C and (b) 1 %w/v L81 with 10 mM cationic surfactants (fixed) as a function of temperature.

The temperature scan in 1 %w/v L81 with 10 mM cationic surfactants reveals the influence of temperature on $D_h$ **(Figure 4b)**. The $D_h$ of the mixed micelles is found to increase slightly with temperature, i.e., from DTAB ~ 19.1 nm (at 30 °C) to ~ 27.4 nm (at 40 °C) to ~ 37.4 nm (at 50 °C) and to ~ 39.8 nm (at 60 °C). For 12-2-12, the $D_h$ values were observed from ~ 25.3 nm (at 30 °C) to ~ 31.0 nm (at 40 °C) to ~ 55.2 nm (at 50 °C) and to ~ 69.7 nm (at 60 °C) **(Figure 4b)**. A similar behavior is observed with 10 mM DDAB, but the increase in the $D_h$ is even more distinct than for the former two surfactants. Thus, as the cationic surfactant becomes more hydrophobic, the temperature effect is more pronounced, favouring the micellar growth and subsequent transition **(Figure 4b)**. This is in qualitative agreement with the phase behavior as shown in **Figure 3**.

The impact of cationic surfactants was also tested on 3 %w/v L81 at 30 ºC and 60 ºC (**Figure 5**). The micellar core and corona get dehydrated at higher temperature and therefore the $D_h$ of the micelles increases from 30 ºC to 60 ºC, probably giving a hint of the micelles undergoing morphological growth/ transition. Furthermore, it was clearly seen that at very low concentration of cationic surfactants (~ 5 mM) the system formed polymer-rich micelles while on increasing concentration of cationic surfactant to 30 mM, the $D_h$ decreases drastically suggesting the copolymer gets solubilized in the cationic surfactant micellar core thereby hinting at the formation of cationic surfactant-rich micelles. Such trend in the size distribution profile endorses the effect of dehydration which may influence the aggregation number ($N_{agg}$) and the micellar core size with a more compact PEO shell.

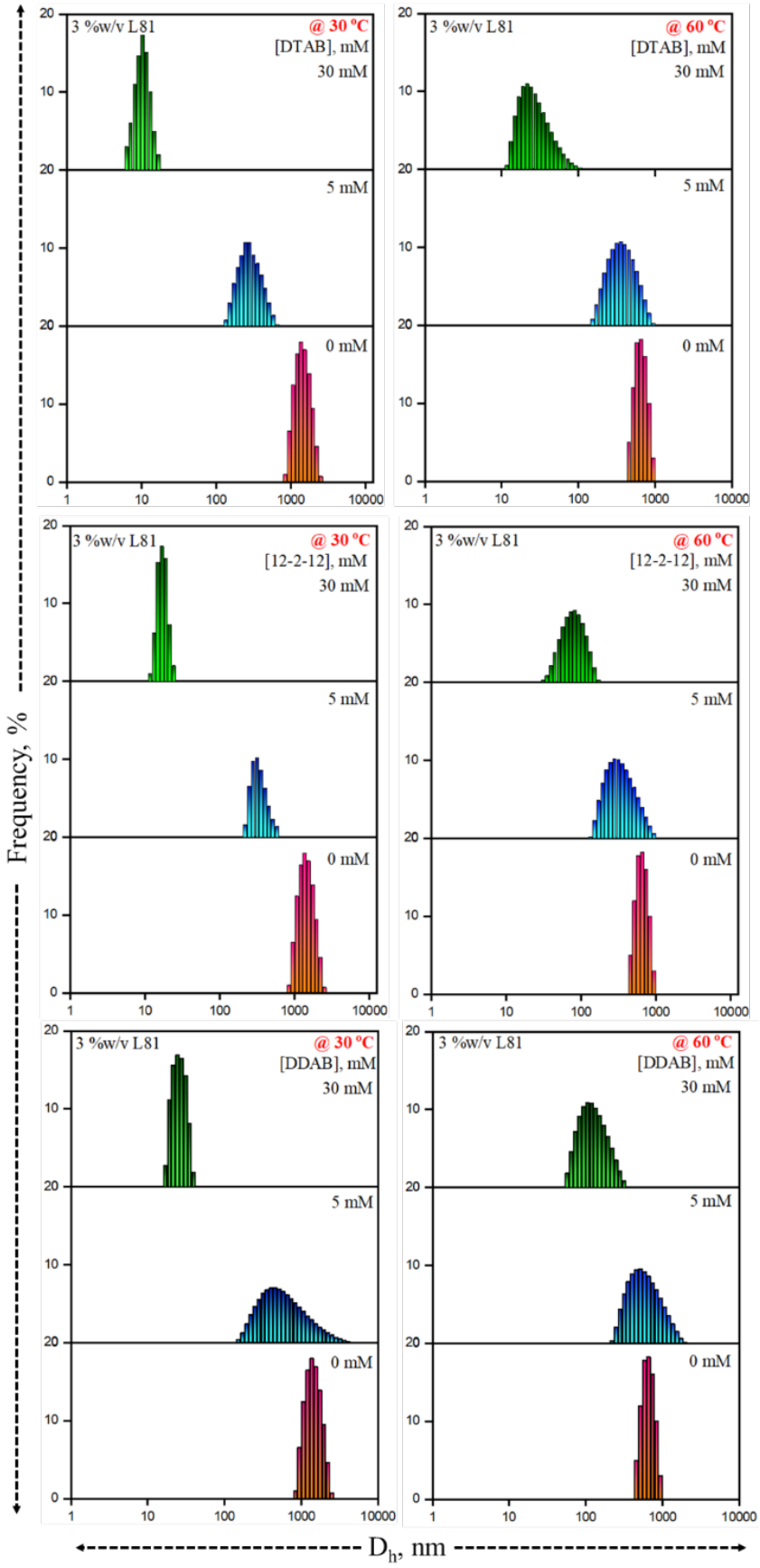


**Figure 5.** The size distribution profile ($D_h$) for 3 %w/v L81 with 5 mM and 10 mM cationic surfactant as a function of temperature.

**SANS analysis**

The solutions were further investigated using SANS to confirm the changes in morphology as a result of the incorporation of cationic surfactants within the polymeric micellar aggregates. The scattering curves of individual components i.e., 1 %w/v L81 (multilamellar vesicles, $R_r$ = 14.57 Å), 10 mM of DTAB (spherical micelles, $R_c$ = 23.9 Å), 10 mM of 12-2-12 (cylindrical micelles, $R_{cr}$ = 37.5 Å, L > 500 Å), and 10 mM of DDAB (multilamellar vesicles with thickness ~20.8 Å and vesicle size $R_v$ > 500 Å of the utilising $Q^{-3}$) in water (on account of SANS, $D_2O$) at 30 °C are presented in **Figure 6.**

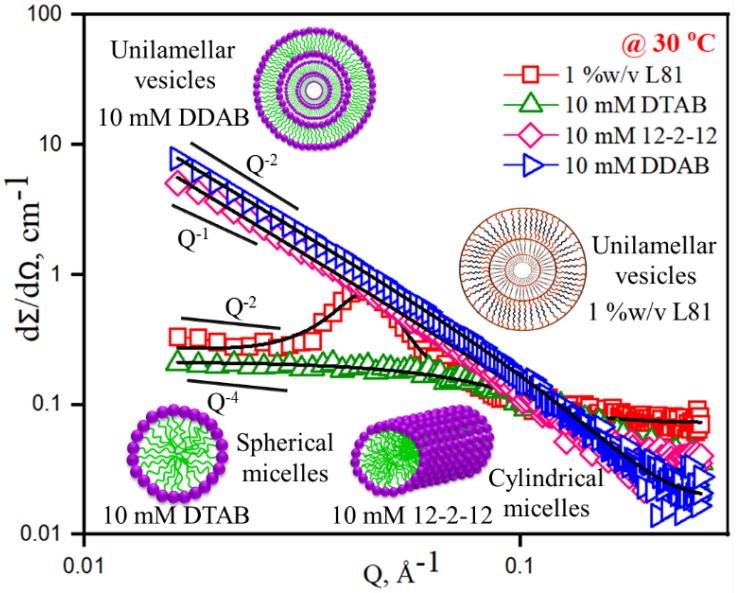


**Figure 6.** SANS data pattern for pure 10 mM surfactants: DTAB, 12-2-12 and DDAB; as well as 1 %w/v Pluronics® L81 at 30 °C.

In the low-$Q$ region of the SANS data for unilamellar vesicles (ULV), the scattering intensity decreased in a straight line as $1/Q^2$ indicating presence of large vesicles. At higher $Q$ values, there was increase in the drop of the intensity and a minimum was observed, which depends on the thickness of the hydrophobic component (monolayer). These ULVs thus were characterized by the monolayer thickness ($t$) as the measurement of the radius of the vesicle ($R_v$) was limited by the $Q_{min}$ of the SANS instrument. The absence of lower cut-offs in the data indicates that the radii of the vesicles could be larger than what could be determined from the present $Q_{min}$ and therefore the radius of the vesicle was kept fixed at a higher value than to a value of $2\pi/Q_{min}$, i.e., ~ 500 Å. On the other hand, in the SANS data from long cylindrical micelles, in the low-$Q$ region of the data, the scattering intensity decreased following a power law as $1/Q$ indicating the formation of long cylindrical micelles. These cylinders were

characterized by the cross-sectional radius ($R_{cr}$) while the measurement of their length ($L$) was limited by the $Q_{min}$ of the instrument.

Previous investigations have revealed the thickness of the unilamellar vesicles to be significantly smaller due to the interdigitating of the hydrophobic tails[16,32,33]. The scattering from the headgroups region is small and can be neglected. It is generally accepted that for the aggregates formed from surfactants, some solvent ($D_2O$) molecules penetrate the headgroup region to some extent, and thus decrease the contrast, thereby reducing the apparent bilayer thickness measured by SANS.

SANS information sheds light on the morphology of L81 micelles upon the addition of cationic surfactants at different temperatures. The results of the SANS experiments revealed that the cationic surfactants greatly impacted the structural features of L81 micelles. Here, we have classified the concentration regimes of cationic surfactants i.e., low (0-3 mM), and high (10-50 mM) to enable a more systematic analysis as presented in **Figure 7**.

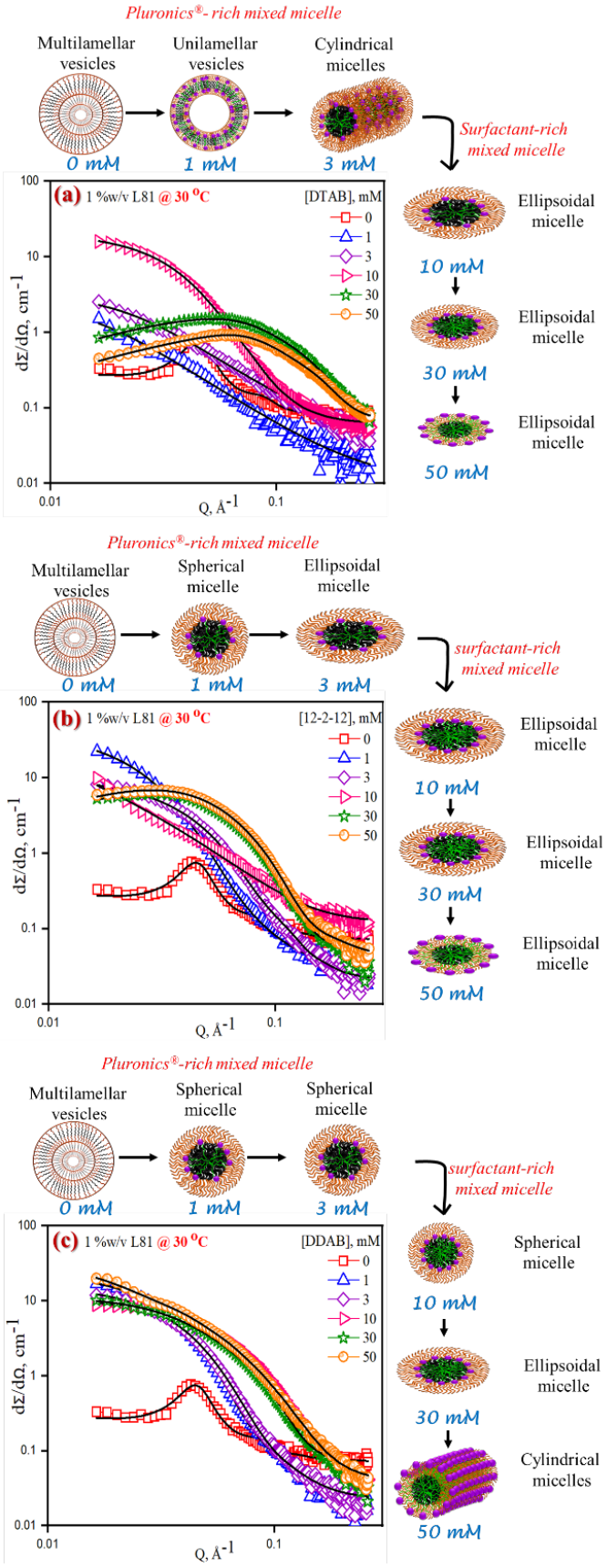


**Figure 7.** SANS curves with the structure factors and associated conformations for 1 %w/v L81 at 30 °C with varying concentration of different cationic surfactants: (a) DTAB; (b) 12-2-12; (c) DDAB.

To begin with, the formation of multilamellar vesicles in the neat 1 %w/v L81 solution was confirmed from the shape of its pair-distance distribution function, p(r) (**Figure 6**). L81-DTAB data shows observable changes in the scattering profile of micelles in the low DTAB regime i.e., the scattering intensity decreases and the correlation peak shifts to a higher Q region (**Figure 7a**). Looking at the calculated structural parameters (**Table 1**), we infer that such reduction in scattering intensity originated from the contraction of the micellar core along with the lowering in the $N_{agg}$ of L81. As a result, the numerical value of scattering length density highlights the contrast existing among core, shell, and dispersion medium ($D_2O$) during data acquisition[29]. As the cationic surfactant concentration increases, the Pluronics® multilamellar vesicles change to unilamellar vesicles at 1 mM DTAB concentration, with size of vesicle ($R_v$) > 500 Å, thickness of vesicle ($t_v$) = 13.2, and then convert into cylindrical micelles at 3 mM, with cross-sectional radius ($R_{cr}$) 19.3 Å, L > 500. As a result, 1 mM to 3 mM DTAB solutions in 1 %w/v L81 show Pluronics®-rich mixed micelles. Further increasing the concentration of DTAB from 10 mM to 50 mM led to the formation of ellipsoidal micelles with increasing ratio of surfactant/Pluronics® aggregation numbers, hence resulting in cationic surfactant-rich mixed micelles (**Figure 7a**) which is well accordance with reported works[16,17].

**Table 1:** Fitted SANS parameters (semi-major axis (a), semi-minor axis (b), hard sphere radius ($R_{hs}$), core radius ($R_c$), radius of gyration ($R_g$), cross-sectional radius ($R_{cr}$) effective charge ($\alpha$), length of rod (L), thickness of vesicle ($t_v$), size of vesicle ($R_v$) and aggregation number ($N_{agg}$) for 1 %w/v L81 with varying concentration of cationic surfactants at 30 °C.

| System | Morphology and parameter | $N_{agg}$ | |
|---|---|---|---|
| **1 %w/v L81** | | | |
| 0 | Multilamellar vesicles, $R_r$ = 14.6 ± 0.06 Å | — | — |
| **1 %w/v L81 + [DTAB], mM** | | | |
| 1 | Unilamellar vesicles, $t_v$ = 13.2 ± 0.05 Å, $R_v$ > 500 Å | — | — |
| 3 | Cylindrical micelles, $R_{cr}$ = 19.3 ± 0.07 Å, $L$ > 500 Å | — | — |
| 10 | Ellipsoidal micelles, $a$ = 87.2 ± 1.5 Å, $b$ = 40.3 ± 0.09 Å | 110 | 301 |
| 30 | Ellipsoidal micelles, $a$ = 30.0 ± 0.08 Å, $b$ = 14.3 ± 0.06 Å, $\alpha$ = 0.21, $R_{hs}$ = 26.3 ± 0.07 Å | 3 | 27 |
| 50 | Ellipsoidal micelles, $a$ = 25.5 ± 0.08 Å, $b$ = 14.5 ± 0.06 Å, $\alpha$ = 0.33, $R_{hs}$ = 37.2 ± 0.09 Å | 2 | 30 |
| **1 %w/v L81 + [12-2-12], mM** | | | |
| 1 | Spherical micelles, $R_c$ = 69.6 ± 1.2 Å | 327 | 89 |
| 3 | Ellipsoidal micelles, $a$ = 60.2 ± 1.1 Å, $b$ = 43.4 ± 0.08 Å | 101 | 83 |
| 10 | Ellipsoidal micelles, $a$ = 228.1 ± 1.9 Å, $b$ = 19.2 ± 0.06 Å | 59 | 161 |
| 30 | Ellipsoidal micelles, $a$ = 72.1 ± 1.3 Å, $b$ = 28.2 ± 0.07 Å, $R_{hs}$ = 35.8 ± 0.08 Å | 25 | 204 |
| 50 | Ellipsoidal micelles, $a$ = 70.6 ± 1.3 Å, $b$ = 28.3 ± 0.07 Å, $R_{hs}$ = 35.8 ± 0.08 Å | 18 | 242 |
| **1 %w/v L81 + [DDAB], mM** | | | |
| 1 | Spherical micelles, $R_c$ = 58.1 ± 1.1 Å | 190 | 52 |
| 3 | Spherical micelles, $R_c$ = 50.4 ± 1.0 Å | 114 | 93 |
| 10 | Spherical micelles, $R_c$ = 28.8 ± 0.07 Å | 17 | 46 |
| 30 | Ellipsoidal micelles, $a$ = 82.8 ± 1.4 Å, $b$ = 26.4 ± 0.07 Å | 25 | 205 |
| 50 | Cylindrical micelles, $R_{cr}$ = 24.6 ± 0.06 Å, $L$ = 267.2 ± 2.1 Å | 38 | 520 |

*Note:* The first $N_{agg}$ value stands for L81 and the second value stands for the surfactant.

Furthermore, micelles did not associate to form large aggregates, most likely as a result of surface charge imparted by DTAB molecules at 30 °C. As stated before, aggregation of charged micelles would depend on the relative concentration of cationic surfactant in the mixed micelles (here estimated via $N_{agg}$ of DTAB) and on the size of the mixed micelles. This implies that higher $N_{agg}$ of DTAB would be conducive to higher effective charge and greater separation among the micelles. The data shown in **Table 1** thus suggest that aggregation of micelles would have been prevented by the appearance of effective charge. DTAB can be seen to lead to saturation in the solubilization ability of L81 micelles and hence to excessive charge build-up in the shell region. As a result, micelles were stabilized to form Pluronics®-rich mixed micelles and cationic surfactant-rich mixed ellipsoidal micelles.

The SANS data of the two other surfactants (12-2-12) and DDAB with L81 followed analogous trends. In (12-2-12), observations include reduction of Pluronics® aggregation (327 to 10) and increase in aggregation number of surfactant (89 to 242) from 1 to 50 mM (**Figure 7b**) at 30 ºC. For DDAB, there is also a decrease of Pluronics® aggregation (190 to 38) and increase in $N_{agg}$ of surfactant (52 to 520) from 1 to 50 mM (**Figure 7c**). To compare the cationic surfactants, the same lengths of the hydrophobic tails increase aggregation number, following the trend: DTAB < (12-2-12) < DDAB due to increasing hydrophobicity of the surfactant.

The SANS data of mixed systems composed of Pluronics® with 10 mM cationic surfactants are shown in **Figure 8** as a function of temperature. The variations in the form of the scattering data of L81 with 10 mM DTAB, as shown in **Figure 8a,** illustrate that the shape of the aggregates is strongly dependent upon the composition of the solution. As the temperature increases from 30 ºC to 60 ºC, we have observed the micellar transition from ellipsoidal micelles to unilamellar vesicles with increasing micellar thickness (**Table 2**). Only the ellipsoid model captured the shape of the mixed aggregates in the measured Q range at 30 ºC. The scattering data at these concentrations have been analysed using the ellipsoid model, considering the intermicellar interactions. This model incorporates the ellipsoidal growth with a minor/major axis ratio, and for aggregation numbers greater than that which will pack into a sphere, the formation of ellipsoids results.

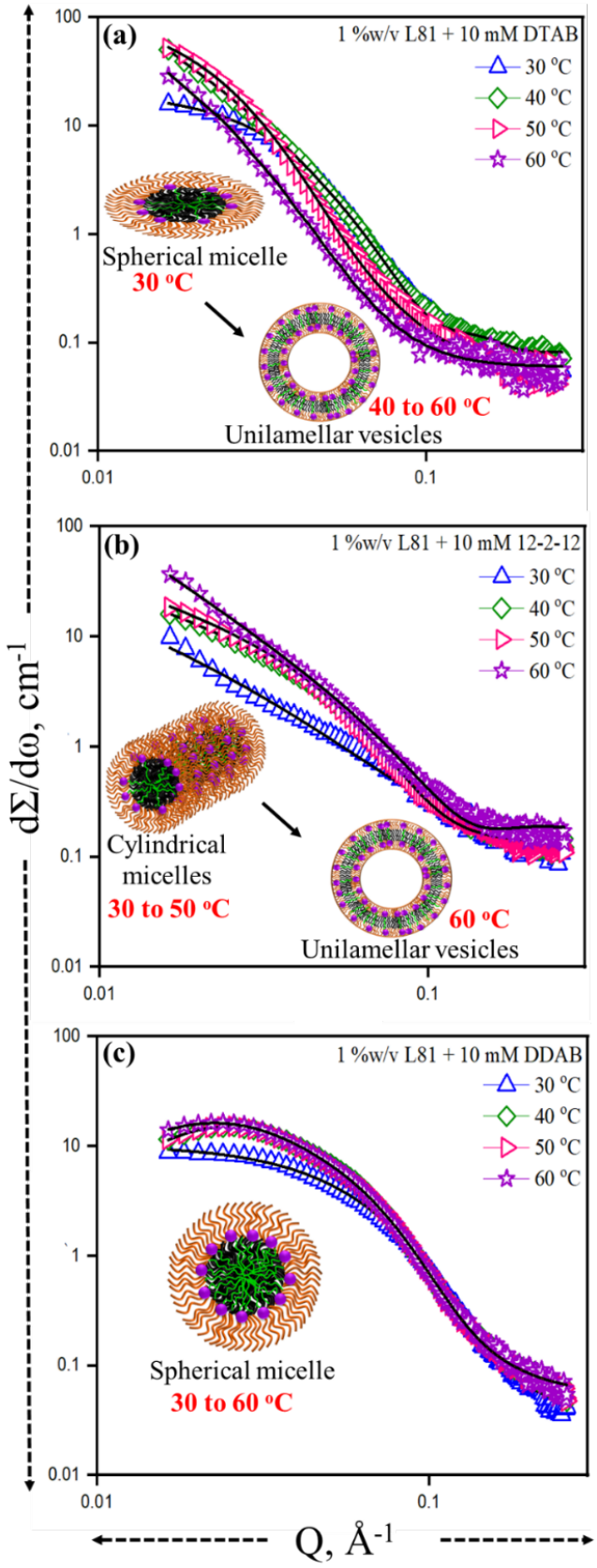


**Figure 8.** Normalized scattering cross-section profile (dΣ/dΩ) as a function of the scattering vector Q along with the schematic clouding behavior for 1 %w/v L81 as a function of temperature with 10 mM cationic surfactants: (a) DTAB; (b) 12-2-12; (c) DDAB.

In the case of (12-2-12), the data shows micellar transitions from ellipsoidal micelles (at 30 °C) to cylindrical micelles (at 40 and 50 °C) to unilamellar vesicles (at 60 °C) with increasing cross-sectional radius (**Figure 8b**). The fitted parameters obtained from the data analysis are shown in **Table 2**. In contrast, in 1 %w/v L81 with 10 mM DDAB, the analysis of scattering data suggests the presence of spherical micelles, which do not significantly change shape as a function of temperature (**Figure 8c**). Although the overall $N_{agg}$ increases somewhat with temperature, the relative proportion of L81/DDAB remains constant at approximately 0.37 (see **Table 2**). This confirms our previous assertion (see **Figure 4**) that temperature causes a slight increase in aggregate size for the DDAB/L81 system, but does not change the morphology of the aggregates.

**Table 2:** Fitted SANS parameters for 1 %w/v L81 with 10 mM different cationic surfactants as a function of temperature.

| System | T, (°C) | Morphology and parameters | $N_{agg}$ | |
|---|---|---|---|---|
| 10 mM DTAB | 30 | Ellipsoidal, $a$ = 87.2 ± 1.5 Å, $b$ = 40.3 ± 0.09 Å | 112 | 304 |
| | 40 | Unilamellar vesicles, $t_v$ = 58.7 ± 1.1 Å, $R_v$ > 500 Å | — | |
| | 50 | Unilamellar vesicles, $t_v$ = 101.7 ± 1.5 Å, $R_v$ > 500 Å | — | |
| | 60 | Unilamellar vesicles, $t_v$ = 148.9 ± 1.7 Å, $R_v$ > 500 Å | — | |
| 10 mM 12-2-12 | 30 | Ellipsoidal micelles, a = 228.1 ± 1.9 Å, b = 19.2 ± 0.06 Å | — | |
| | 40 | Cylindrical micelles, $R_{cr}$ = 30.7 ± 0.07 Å, $L$ > 500 Å | — | |
| | 50 | Cylindrical micelles, $R_{cr}$ = 34.1 ± 0.08 Å, $L$ > 500 Å | — | |
| | 60 | Unilamellar vesicles, $t_v$= 38.5 ± 0.08 Å, $R_v$ > 500 Å | — | |
| 10 mM DDAB | 30 | Spherical micelles, $R_c$ = 28.8 ± 0.07 Å | 17 | 46 |
| | 40 | Spherical micelles, $R_c$ = 32.7 ± 0.08 Å, $\alpha$ = 0.32, $R_{hs}$ = 43.4 ± 0.09 Å | 25 | 67 |
| | 50 | Spherical micelles, $R_c$ = 34.7 ± 0.08 Å, $\alpha$ = 0.29, $R_{hs}$ = 45.9 ± 0.1 Å | 29 | 80 |
| | 60 | Spherical micelles, $R_c$ = 35.1 ± 0.08 Å, $\alpha$ = 0.24, $R_{hs}$ = 47.7 ± 0.1 Å | 30 | 83 |

*Note:* The first $N_{agg}$ value stands for L81 and the second value stands for the surfactant.

**Figure 9** shows a higher scattered intensity due to the formation of micelles in the 3 %w/v L81 solution. SANS data for solutions of cationic surfactant with varying concentrations are given in **Table 3**. Lower scattered intensity is attributed to the unimer in solution[53,64]. The increase in the scattered intensity can be understood in terms of change in the contrast $(\rho_m - \rho_s)^2$ between the micelle and the solvent. However, an increase in neutron-scattering intensity is due to an increase in the size of the PPO core. Upon addition of increasing concentration of cationic surfactant (5 mM to 30 mM) the micelle size decreases as the addition of cationic surfactant destroys the aggregates of L81. Due to the hydrogen bond and hydrophobic interactions between L81 and cationic surfactant, surfactant cations align within the L81 micelles to form mixed micelles. On the one hand, this enhances the electrostatic repulsion between PEO groups of L81 and on the other hand, due to the preferential partitioning in the

hydrophobic region, the surfactants will interact with dehydrated PPO blocks. Therefore, electrostatic repulsion opens up the micelle and the tail chains of surfactant molecules permeate into PPO block and remove L81 monomer, thus decreasing the size of micelles. These results are in agreement with the DLS study (**Figure 5**).

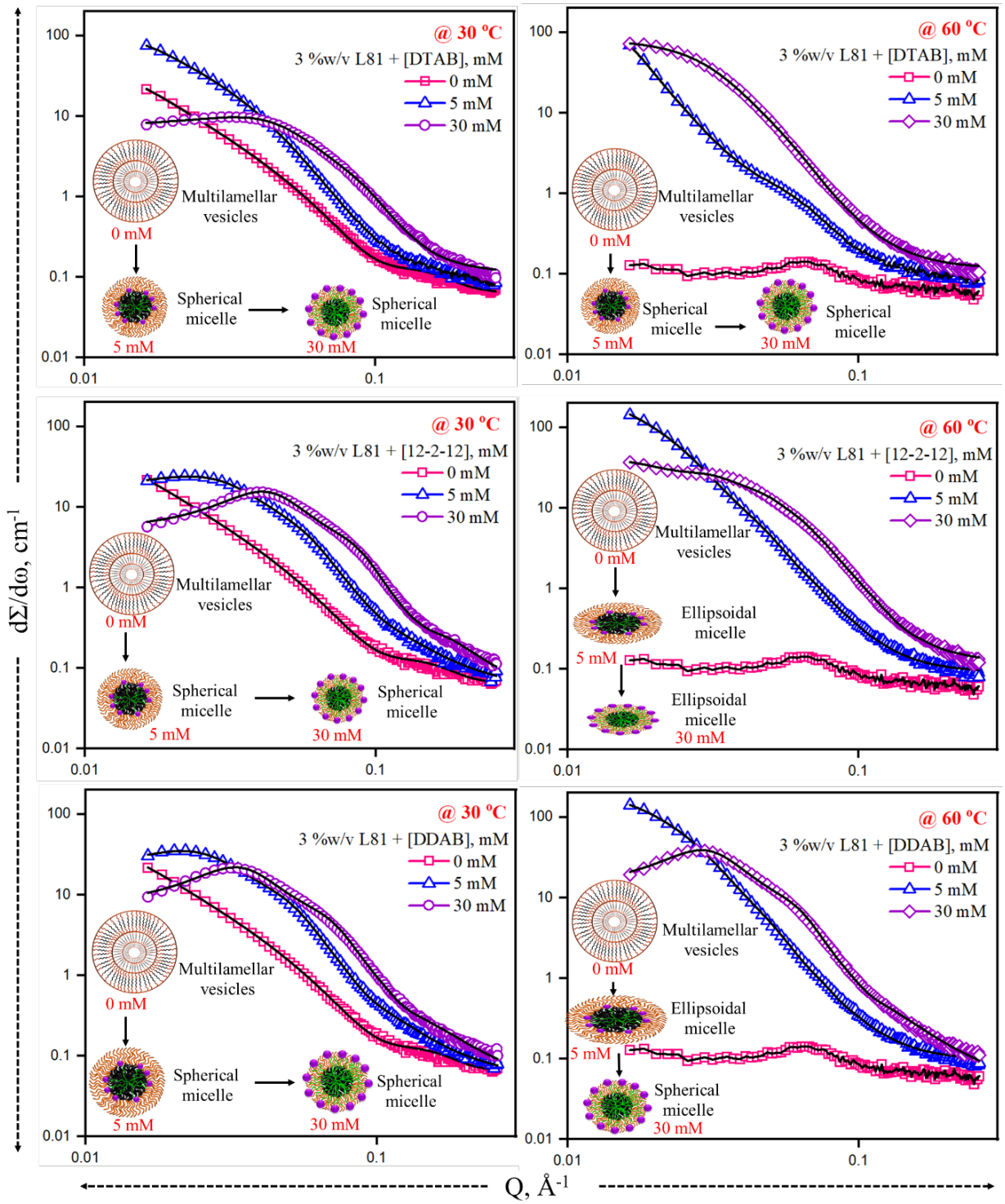


**Figure 9.** Normalized scattering cross-section profile (dΣ/dΩ) as a function of the scattering vector Q along with the schematic clouding behavior for 3 %w/v L81 with 5 mM and 30 mM cationic surfactant as a function of temperature.

Furthermore, 3 %w/v L81 at 30 °C contains unilamellar vesicles with thickness $t_v$ = 56.0 Å, while with increasing temperature at 60 °C it aggregates. The intensity of the scattering is reduced in the presence of 5 mM cationic surfactants (DTAB, 12-2-12, DDAB); the micelles are spherical with $N_{agg}$ 230 and 103, spherical with $N_{agg}$ 78 and 35, and spherical with $N_{agg}$ 104 and 46, respectively at 30 °C. This means that, interestingly, the surfactant/L81 ratio in the mixed micelles is approximately the same for all three surfactants at this concentration. Both the 12-2-12 and DDAB systems (but not DTAB) exhibit micellar transitions from spherical to ellipsoidal with increasing $N_{agg}$ with increasing temperature from 30 to 60 °C. It is clearly seen that as the concentration of surfactant increases, the $N_{agg}$ and the micellar size decreases because of the above-mentioned transition from Pluronics®-rich to cationic surfactant-rich mixed micelles which agrees very well with the published study[17].

**Table 3:** Fitted SANS parameters for 3 %w/v L81 with 5 mM and 30 mM different cationic surfactants as a function of temperature.

| System | T, (°C) | Morphology and parameters | $N_{agg}$ | |
|---|---|---|---|---|
| **3 %w/v L81** | | | | |
| 0 | 30 | Unilamellar vesicles, $t_v$ = 56.0 ± 1.0 Å, $R_v$ > 500 Å | — | |
| **3 %w/v L81 + [DTAB], mM** | | | | |
| 5 | 30 | Spherical, $R_c$ = 61.8 ± 1.2 Å | 230 | 103 |
| | 60 | Spherical, $R_c$ = 31.0 ± 0.08 Å | — | |
| 30 | 30 | Spherical, $R_c$ = 30.7 ± 0.08 Å, $R_{hs}$ = 64.6 ± 1.2 Å | 24 | 64 |
| | 60 | Spherical, $R_c$ = 57.8 ± 1.1 Å, $R_{hs}$ = 94.5 ± 1.3 Å | 159 | 426 |
| **3 %w/v L81 + [12-2-12], mM** | | | | |
| 5 | 30 | Spherical, $R_c$ = 43.5 ± 0.09 Å, $R_{hs}$ = 99.2 ± 1.3 Å | 78 | 35 |
| | 60 | Ellipsoidal, $a$ = 130.6 ± 1.5 Å, $b$ = 48.4 ± 0.1 Å | 288 | 129 |
| 30 | 30 | Spherical, $R_c$ = 30.5 ± 0.07 Å, $R_{hs}$ = 68.0 ± 1.1 Å | 20 | 54 |
| | 60 | Ellipsoidal, $a$ = 58.2 ± 0.09 Å, $b$ = 27.5 ± 0.07 Å | 31 | 83 |
| **3 %w/v L81 + [DDAB], mM** | | | | |
| 5 | 30 | Spherical, $R_c$ = 47.9 ± 0.09 Å, $R_{hs}$ = 115.5 ± 1.4 Å | 104 | 46 |
| | 60 | Ellipsoidal, $a$ = 128.8 ± 1.5 Å, $b$ = 55.6 ± 1.1 Å | 375 | 168 |
| 30 | 30 | Spherical, $R_c$ = 35.7 ± 0.07 Å, $R_{hs}$ = 85.0 ± 1.3 Å | 32 | 86 |
| | 60 | Spherical, $R_c$ = 41.7 ± 0.08 Å, $R_{hs}$ = 95.7 ± 1.4 Å | 51 | 137 |

*Note:* The first $N_{agg}$ value stands for L81 and the second value stands for the surfactant.

As shown in **Figure 9**, the addition of cationic surfactant causes a decrease in scattering profile indicating a higher degree of Pluronics®/ ionic surfactant interaction responsible for demicellization. The decrease in aggregation number was evidenced, confirming the role of chain length of cationic surfactant. Due to preferential partitioning in the hydrophobic region, cationic surfactants will interact with the dehydrated PPO blocks. In other words, long chain incorporation into the micelle core drives out copolymer monomers, which is responsible for the decrease in size.

**CG-MD simulations**

As described in the previous section, the behavior of L81 in aqueous phase is considerably affected upon addition of the cationic surfactants. Thus, the impact DTAB, DDAB and 12-2-12 in the L81 aggregation in aqueous solution was further analysed through CG-MD simulations. It should be noted at the outset that, due to limitations on the size and length scales of the systems accessible to CG-MD simulations with explicit solvent, it is difficult to quantitatively replicate the conditions of the experimental work (particularly those used in SANS measurements). Hence, we aim primarily to draw a qualitative comparison and gain insight into the physical mechanisms governing self-assembly and interactions between the different components of the system. Concretely, we used 3 %w/v Pluronic instead of 1 %w/v since the latter was too diluted to observe a meaningful aggregation within a reasonable computational time. For the same reason, we ran surfactant concentrations between 5 and 90 mM. The L81 aqueous solution at 3 %w/v concentration (run 5) was taken as a reference, and it was run for 1000 ns. This system quickly formed a single L81 aggregate as noticed in the simulation snapshot shown in **Figure 10a**. The density profile was obtained with the cluster counting code where the density of selected CG beads was displayed from the micelle centre of mass (CoM) as shown in **Figure 10b**. The density profile shows a spherical aggregate with an estimated radius of ~ 2.5 nm. Given the relatively small size of the simulation boxes (already at the limit of what can be reasonably achieved with present computational resources), we would not expect the L81 solution to form complete vesicles during the simulation. Instead, the outcome simply suggests that the equilibrium aggregation number for this system is larger than 50.

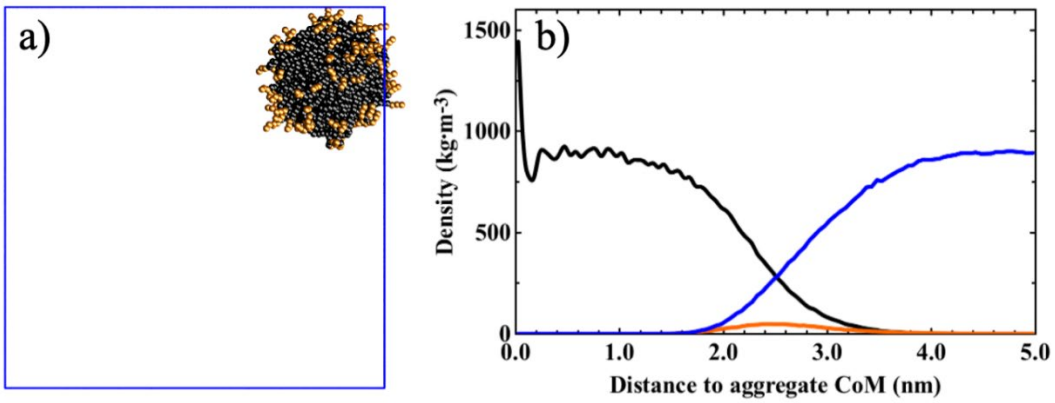


**Figure 10.** a) CG-MD simulation snapshot for the 3 %w/v of L81 aqueous solution at 333K. b) density profile of the obtained aggregate taking the centre of mass (CoM) as reference. The colour code is as follows; the PEO and PPO groups in the L81 were coloured in orange and black, respectively, and water is in blue. The water molecules in the simulation snapshot (a) were removed for clarity.

*L81/DTAB/Water mixture*

A set of four CG-MD simulations was prepared (runs 6, 7, 8 and 9 described in **Table S1**, of Supplementary Information) considering four DTAB concentrations (5, 10, 30 and 90 mM) to analyse the impact of DTAB concentration on L81 aggregates and to shed light into the results shown in the experimental section. The systems were equilibrated and run for 1000 ns where the last simulation snapshots for each system are displayed in **Figures 11a, c, e, and g**. At 5 mM of DTAB concentration, the L81 quickly formed a single aggregate like in L81 aqueous solution (run 5), reflecting a weak impact of the relatively few DTAB molecules present. **Figure 11b** displays the density profile of L81 aggregates with adsorbed $DTA^+$ and $Br^-$ at the surface (see the green and purple DTAB peaks around the L81 PEO peak coloured in orange). Similar behavior was found when the DTAB concentration was increased to 10 mM. The DTAB molecules were arranged at the L81 surface as illustrated in the simulation snapshot shown in **Figure 11c** and noticed in the density profile shown in **Figure 11d**. Conversely, with 30 mM DTAB, the system exhibited smaller L81/DTAB micelles as shown in **Figure 11e**. Thus, the increase in available DTAB molecules promoted an increased interaction with L81 in the initial stages of the self-assembly and therefore increased the charge density on L81 micelle surface. This could be the reason behind the formation of smaller micelles as also noticed in mixtures of aqueous solutions of Pluronic® and ionic liquids[19,24,61,62]. According to these results, the observed behavior suggests that repulsive inter-micelle interactions that play the main role in the self-assembly, hindering the formation of larger L81 aggregates. The L81 system with 5 mM and 10 mM DTAB displayed a micelle surface charge of 0.20 and 0.38 $nm^{-2}$, respectively, whereas 0.7 $nm^{-2}$ was observed in the 30 mM mixture. As expected, the impact was more evident when the DTAB concentration was increased to 90 mM where more L81/DTAB micelles were formed displaying a L81 micelle surface charge of 1.2 $nm^{-2}$ (**Figure 11g**).

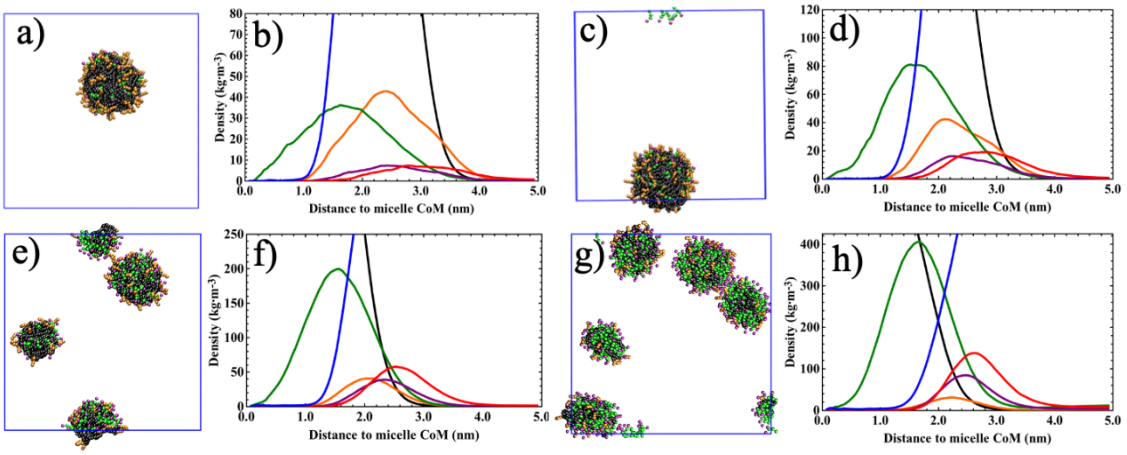


**Figure 11.** CG-MD simulation snapshots, with the density profiles focused on the micelle surface, for the 3 %w/v L81 aqueous solution with four DTAB concentrations; (a, b) 5 mM, (c, d) 10 mM, (e, f) 30 mM and (g, h) 90 mM. The colour code is as follows: PEO and PPO in the L81 Pluronic® are in orange and black, respectively. The DTAB alkyl tail and charged head group are in green and purple, respectively. Water is plotted in blue and bromide counterions in red colour; both were removed in the simulation snapshots for clarity.

In fact, at 90 mM DTAB, the mixture exhibited more micelles (**Figure 11g**) but the average diameter – roughly estimated by the maximum of the L81 PEO peak shown in orange in **Figure 11h** – was greater than the micelles (**Figure 11e**) obtained in the 30 mM DTAB mixture (**Figure 11f**). This reflects the different self-assembly mechanisms that dominate as the cationic surfactant concentration increases. By analysing the CG-MD trajectories, the micelle formation can be explored at different self-assembly stages. **Figures S1a-d** show the aggregation process at every 200 ns of simulation time for all DTAB concentrations. In the first 200 ns, the initial stages of self-assembly at the three lowest concentrations were dominated by formation L81 aggregates, onto which DTAB molecules adsorbed. In contrast, in the 90 mM mixture, the DTAB micelle formation competed with formation of L81 aggregates, with some L81 monomers even adsorbing onto DTAB micelles. In fact, in the first 200 ns, the 90 mM system was the only one displaying isolated DTAB micelles. In the next stages of the simulation, the 5, 10 and 30 mM behaved similarly with L81 micelles dominating the aggregation and adsorbing DTAB moieties, especially noticeable in the 30 mM system, since more DTAB are available but not enough to form isolated DTAB micelles.

In summary, the MD simulations results for this system infer a relative gradual transition from Pluronic-rich to cationic surfactant-rich aggregation as the surfactant concentration is increased. Furthermore, at low ionic surfactant concentrations, the self-assembly process does not seem to be much affected by the presence of ionic surfactant, with aggregates resembling those formed in the pure L81 solution.

*L81/12-2-12/W mixture*

Four 12-2-12 concentrations (5, 10, 30 and 90 mM) were added to the 3 %w/v L81 aqueous solution and simulated by CG-MD (runs 10, 11, 12 and 13 in **Table S1**). **Figures 12a, c, e, and g** display the last simulation snapshots for each system after 1000 ns. At 5 mM, the L81 quickly forms two micelles, the density profile of which is shown in **Figure 12b**, with adsorbed 12-2-12 molecules at the L81 micelle surface. For the 10 mM system, only one L81 micelle with adsorbed 12-2-12 was formed as shown in **Figure 12c**. Thus, the L81 still dominated the aggregation and the 12-2-12 molecules seemed to cooperate in the L81 micelle formation. The increased charge density of the micelle surface from 0.3 $nm^{-2}$ in 5 mM to 0.7 $nm^{-2}$ in the 10 mM solution was not a barrier for micelle growth, and the hydrophobic strength of the double alkyl tail seemed to overcome any inter-micelle repulsions due to the increased density of charge. The micelle density profile is shown in **Figure 12d** where all 12-2-12 headgroups were arranged close to the L81 PEO groups at the micelle surface. Conversely, the 30 mM 12-2-12 mixture exhibited two micelles, as shown in **Figure 12e**, where the surfactant was more noticeable compared with lower concentrations. At 30 mM, the charged 12-2-12 head groups seemed to overcome the double alkyl tail hydrophobic contribution in the self-assembly, exhibiting an increased micelle density of charge of 1.3 $nm^{-2}$. The 30 mM system yielded two micelles, like the 5 mM system, but the micelles were more voluminous as can be noticed in the micelle density profile shown in **Figure 12f**. Furthermore, more 12-2-12 can be found out of the micelle surface as can be seen if one compares the charged head groups (purple peak) in both the 5 mM and 30 mM profiles. Thus, between 10 and 30 mM of 12-2-12 concentration, we found a threshold in the L81 micelle formation likely related with two competing forces: hydrophobic *vs* electrostatic interactions at the surface. Finally, **Figure 12g** shows the aggregates obtained in the 90 mM mixture with a clear dominance of 12-2-12, where the L81 moieties were adsorbed before having any chance to form separate micelles. The aggregate shown at the bottom right of **Figure 12g** is a folded micellar rod. The density profile is shown in **Figure 12h** with the wider curves reflecting the fact that rod-like aggregates were formed.

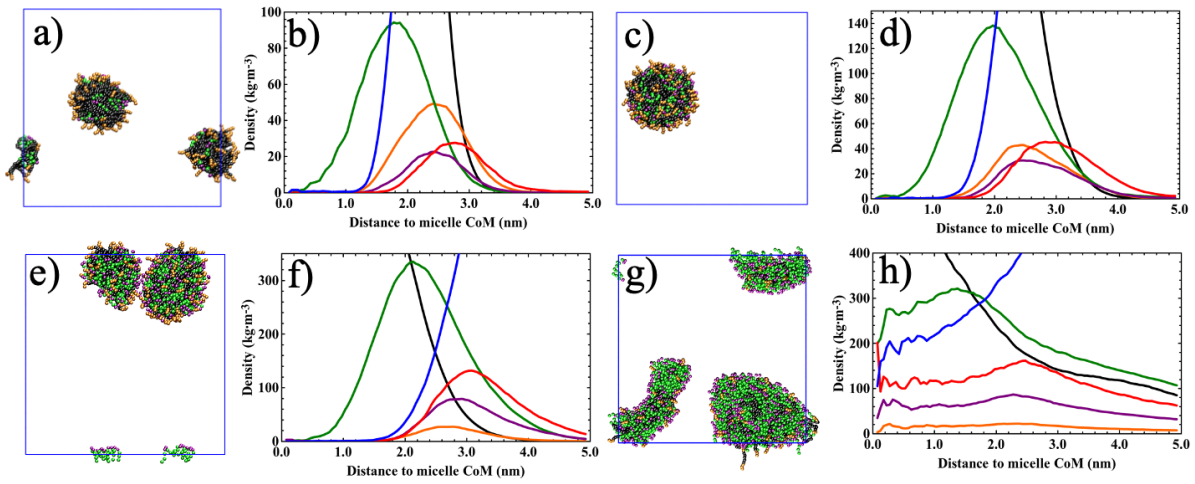


**Figure 12.** CG-MD simulation snapshots, with the density profiles focused on the micelle surface, for the 3 %w/v L81 aqueous solution with four 12-2-12 concentrations; (a, b) 5 mM, (c, d) 10 mM, (e, f) 30 mM and (g, h) 90 mM. The colour code is the same as in **Figure 11**. Water and bromide counterions were removed in the simulation snapshots for clarity.

To understand the complex micelle formation scenario displayed in **Figure 12** with the conflicting impact of the hydrophobic and charge contributions of 12-2-12 in the L81 self-assembly, the initial stages of micelle formation were analysed. The simulation snapshots at every 200 ns of simulation time for 5 mM, 10 mM, 30 mM and 90 mM 12-2-12 concentrations are shown in **Figure S2**. In the initial stage of aggregation of the 5 mM system (**Figure S2a**), the L81 clearly dominated the aggregation where the 12-2-12 monomers were adsorbed onto L81 aggregates. Then, in the first 200 ns, the L81 initial small aggregates grew to form four micelles which were relatively stable until 600 ns with the formation of two micelles which were stable during the next 400 ns. It is likely that these two micelles will fuse to form a single aggregate at equilibrium, given sufficient simulation time. Conversely, in the initial stages of the 10 mM system (**Figure S2b**), some 12-2-12 small aggregates were formed and coexisted with the L81 aggregates. However, after 200 ns, three L81 micelles with all 12-2-12 adsorbed were stable until 600 ns, finalising with micelle fusion into a single aggregate in the next 400 ns. By comparing the dynamics of the micelle distribution along the 1000 ns of simulation for the 5 mM and 10 mM systems, the micelle fusion processes proceeded faster in the more concentrated system if one compares the micelle distributions between 200 and 600 ns displayed in **Figures S2a-b**. For the 30mM solution, **Figure S2c** shows a similar scenario when compared with the 10 mM system but the formation of 12-2-12 micelles in the initial stages was more evident. Over 1000 ns, the 30 mM system displayed more micelles when compared with the 10 mM solution, suggesting that inter-micelle repulsions – due to increased micelle surface charge density – began to play an important role in the aggregation process. At 90 mM,

the initial stage was dominated by formation of 12-2-12 micelles, as clearly illustrated in **Figure S2d,** where only a few L81 moieties were able to form some small aggregates with no more than two or three monomers each. After 200 ns, the system already formed micellar rods with adsorbed L81 as expected in a pure 12-2-12 aqueous solution (**Figure 2d**), and those remained stable along the next 800 ns.

Hence, the MD results for this solution also show a clear transition from Pluronic-rich to cationic surfactant-rich aggregates, as observed in the solution with DTAB. However, the 12-2-12 surfactant seems to exert a stronger effect at low concentrations, leading to the formation of smaller aggregates than in the pure L81 solution, or at least to a significant slow-down of the dynamics of micelle fusion. Furthermore, the 12-2-12 surfactant seems to promote the formation of rod-like, or at least elongated structures at high surfactant concentration. Given the limited time and length scales of the simulations, it is not completely clear if these represent true equilibrium structures or transient structures that would evolve, say, towards larger vesicles as seems to be implied by the analysis of SANS data.

*L81/DDAB/W mixture*

Four simulations (runs 14, 15, 16 and 17 in **Table S1**) were carried for the 3 %w/v L81 aqueous solutions with four DDAB concentrations (5, 10, 30 and 90 mM). The CG-MD simulation snapshots after 1000 ns are shown in **Figure 13a, c, e, and g**. At 5 mM, the L81 quickly formed two micelles with adsorbed DDAB (**Figure 13a**) as was also observed in the 5 mM 12-2-12 system (**Figure 13a**) but different to the 5 mM DTAB system (**Figure 11a**) where a single micelle was formed after 1000 ns. Thus, even at low DDAB surfactant concentration, the charge density of the surfactant head groups seems to impact the L81 aggregation. The micelle density profile displayed in **Figure 13b** shows a similar surfactant arrangement around the micelle surface as in the 12-2-12 and DTAB solutions, where the cationic head groups (purple) were placed close to the L81 PEO groups (orange). At 30 mM, the L81 still dominates the aggregation exhibiting a L81 micelle with adsorbed DDAB, as was found in the 12-2-12 and DTAB 10 mM mixtures shown in **Figure 13c and 11c**, respectively. However, the density profile shown in **Figure 13d** highlights the fact that the DDAB charged head groups were arranged further inside the L81 micelle surface delimited by the PEO groups coloured in orange. This suggests that the double alkyl tail facilitates the arrangement (more hydrophobic) of DDABs in the L81 micelle core, in contrast to the lower hydrophobic strength of DTAB, whilst the lower charge density of the DDAB head group facilitates this task when compared with the 12-2-12. The DDAB increased hydrophobicity and lower head group charge density

character became more pronounced at 30 mM. **Figure 13e** shows the obtained micelle, which basically consists of DDABs with adsorbed L81 moieties as was observed in the DTAB system (**Figure 11e**) but different to the 12-2-12 (**Figure 12e**) where two micelles were obtained. This reflects the fact that the head group charge density played the main role in the aggregation process in the 12-2-12 system as pointed out previously. In the DDAB, the lower charge density of the head group yields the same scenario as in the DTAB; in other words, the DDAB is more like DTAB when compared with the 12-2-12. The micelle density profile of the DDAB 30 mM is shown in **Figure 13f** where the wider curves point towards a prolate-shaped micelle with the DDAB alkyl tails well inside the core. In fact, the peaks observed at ~ 0 (micelle CoM) mean that the prolate-shaped aggregate is a proto-vesicle, since bromides (red) and DDAB head groups (purple) are found at the CoM (red and purple maximum peaks at ~ 0). When the DDAB concentration is increased to 90 mM, the ionic surfactant clearly dominates the aggregation, displaying a large rod-like aggregate basically formed by DDABs with adsorbed L81 as shown in **Figure 13g**. At this high concentration, the DDAB behaves more like a 12-2-12 surfactant since a similar aggregate was found (**Figure 12g**). Nevertheless, the density profile shown in **Figure 13h** clearly describes a rod-like vesicle since not only bromides and DDAB head groups are found in the CoM – red and purple, respectively – but also water and L81 PEO groups – blue and orange, respectively.

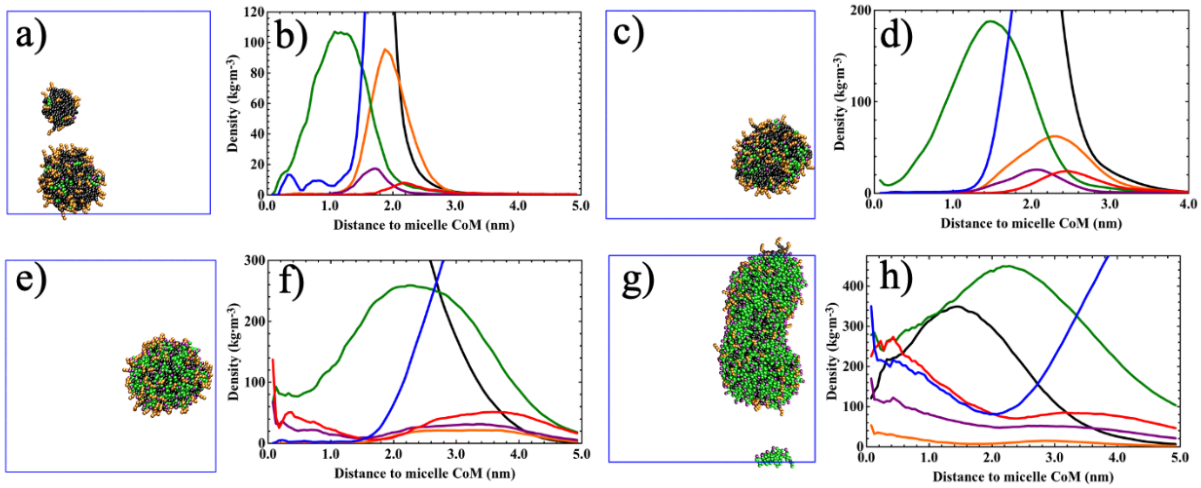


**Figure 13.** CG-MD simulation snapshots, with the density profiles focused on the micelle surface, for the 3 %w/v L81 aqueous solution with four DDAB concentrations; (a, b) 5 mM, (c, d) 10 mM, (e, f) 30 mM and (g, h) 90 mM. The colour code is the same as in **Figure 11**. Water and bromide counterions were removed in the simulation snapshots for clarity.

A detailed analysis of the aggregation processes at different stages is shown in **Figure S3**. At 5 and 10 mM (**Figures S3a-b**) the L81 governed the aggregation with the formation of early micelles where the DDAB monomers were adsorbed completely in the first 200 ns before

any chance to form surfactant micelles. Then, the L81 micelle growth proceeded by fusion processes, similarly in both systems, being the micellization slightly slower in the 5 mM system in which two micelles remained in solution but only one in the 10 mM system. At 30 mM, there was a clear competition between the L81 and DDAB micelle formation as can be seen in the first snapshot of **Figure S3c**. In a first stage, the L81/DDAB and DDAB/L81 micelles coexisted, quickly forming L81/DDAB hybrid micelles after 200 ns. Above 400 ns, all micelles were unified in one rod-like vesicle, as shown by the density profile in **Figure 13f**, which was stable for the next 600 ns. When the DDAB concentration was raised to 90 mM, the DDAB clearly dominated the micelle formation in the initial stage as can be seen in **Figure S3d**. However, the L81 still formed some small aggregates, but they were completely adsorbed by the DDAB micelles in the first 200 ns. Then, a quick micelle fusion yielded a rod-like vesicle which remained stable for the next 600 ns.

Thus, main conclusion that can be extracted from the CG-MD simulations is that the hydrophobicity of the alkyl tails and the density of charge of the head groups had a significant impact on the L81 aggregation. The dilute aqueous solution of the studied surfactants displayed spherical micelles, rod-like micelles, and vesicles for DTAB, 12-2-12 and DDAB, respectively, as in the experiments. This diverse behavior, related to the hydrophobic *vs* head group charge density balance, was translated in different structures, depending on the surfactant concentration; from L81/DTAB (5-10 mM) or DTAB/ L81 (30-90 mM) micelles to L81/12-2-12 (5-10 mM) spherical micelles or 12-2-12/L81 (30-90 mM) rod-like structures or L81/DDAB (5-10 mM) spherical micelles or DDAB/L81 (30-90 mM) vesicles. Thus, above 10 mM of surfactant concentration, in all studied systems, the surfactant overcame the L81 aggregation dominance, but slight differences were also found at lower concentrations. A brief visual analysis of the simulation snapshots displayed in **Figures S1-S3** reveals that the DTAB yielded smaller micelles compared with the 12-2-12 solutions, being the micelle size distribution of DDAB in between them. The double alkyl tail and double head group charge displayed by the 12-2-12 produced bigger aggregates overall whereas the double alkyl tail/single charge head group promoted the formation of vesicles with aggregates slightly smaller compared with those found in the 12-2-12 solutions. Finally, the single alkyl-tail/single-head group charge of DTAB yielded spherical micelles over all concentrations with a decreased micellar distribution size as soon as the ionic surfactant concentration is increased, in agreement with cloud point measurements of Pluronic® aqueous solutions with ionic liquids[37].

## CONCLUSIONS

The present study focuses on the phase behavior and micellization conduct of L81 in the presence of cationic surfactants (DTAB, 12-2-12, and DDAB) investigated from different techniques. The difference in the interactions of these ionic surfactants with Pluronics® L81 stems from the dissimilarities in the size/ structure and hydration of the headgroups. This influences the clouding behavior of L81. i.e., the CP of L81 gets influenced (delayed) dramatically in the presence of the cationic surfactants which is attributed to the hydrogen-bond interactions between the cation of the ionic surfactant and PEO units of L81 and the induced hydrophobic interactions between the alkyl chain of the cationic surfactant and the hydrophobic chain of L81. The dynamic light scattering (DLS) results showed the micelle size decrease as the electrostatic repulsion between PEO groups of L81 is increased due to the permeation of cationic surfactant and forms small scale aggregates. The presence of cationic surfactant within the micelles results enhanced the polarity with significantly altering CP, micelle size and aggregation number. Furthermore, structure of the headgroups of surfactants and the hydrophobic character of Pluronics® affect the structure of the final micellar aggregates. This has been probed from small-angle neutron scattering (SANS) analysis where the composition dependence of the mixed aggregates is depicted quantitatively to derive the micellar shape parameters. Such trend is attributed to the incorporation of cationic surfactant correlated with the appearance of positive charge adsorbed at the surface of L81 micelles which induced micellar transitions. i.e., at low concentration (≤ 3 mM), cationic surfactant stimulated the formation of smaller Pluronics®-rich mixed micelles in higher number while at its high concentrations (50 mM) it formed cationic surfactant-rich mixed micelles. Experimental finding explaining the effect of cationic surfactants on the behavior of Pluronic® in aqueous solution were further corroborated employing molecular dynamics simulations the approach was able to reproduce the micelle distribution experimentally obtained as well as the micelle shapes. Overall, the study here reported offered a fresh insight into the aggregation behavior of hydrophobic Pluronics® L81 in the presence of cationic surfactants to form mixed micellar systems that may turn out to be fairly useful in many applications involving micellar media.

## ACKNOWLEDGEMENT

The authors acknowledge Sardar Vallabhbhai National Institute of Technology (SVNIT), Gujarat, India for providing the instrumentation facilities. The computational part of this work was funded by CICECO-Aveiro Institute of Materials under the projects UIDB/50011/2020, UIDP/50011/2020 & LA/P/0006/2020 and financed by national funds

through the FCT/MEC (PIDDAC). G. Pérez-Sánchez acknowledges national funds (OE), through FCT – Fundação para a Ciência e a Tecnologia, I.P., in the scope of the framework contract foreseen in the numbers 4, 5 and 6 of the articles 23, of the Decree-Law 57/2016, of August 29th, changed by Law 57/2017, of July 19th.

**DECLARATION OF COMPETING INTEREST**

The authors declare that they have no known competing financial interests or personal relationships that could have appeared to influence the work reported in this paper.

**THE ETHICS STATEMENT**

No human or animal subjects were used in this research.

**REFERENCES**

1. Bakshi, S.; Sachar, S. Influence of hydrophobicity on the mixed micelles of Pluronic F127 and P103 plus cationic surfactant mixtures. *Colloids Surf. A Physicochem. Eng. Asp.* **2006**, 276 (1), 146-154.
2. Banipal, S.; Sood, K.; Kaur, J.; Singh, K. Singh, Mixed Micellization Behavior of 12-2-12 Gemini Surfactant with Some Alkyltrimethylammonium Bromide Surfactants. *J Dispers. Sci. Technol.* **2011**, 32 (6), 881-887.
3. Mahajan, K.; Kaur, R.; Aswal, K. Effect of urea on the aggregation behavior of gemini surfactants and their mixed micelles with Pluronic L64. *Colloids Surf. A Physicochem. Eng. Asp.* **2013**, 419, 61-68.
4. Singla, P.; Singh, O.; Sharma, S.; Betlem, K.; Aswal, V.; Peeters, M.; Mahajan, K. R. Temperature-Dependent Solubilization of the Hydrophobic Antiepileptic Drug Lamotrigine in Different Pluronic Micelles-A Spectroscopic, Heat Transfer Method, Small-Angle Neutron Scattering, Dynamic Light Scattering, and in Vitro Release Study. *ACS Omega*. **2019**, 4 (6), 11251-11262.
5. Banerjee, B.; Paria, S. Effect of Electrolytes on Solution and Interfacial Behaviors of Double Chain Cationic-Nonionic Surfactant Mixtures for Hydrophobic Surface Wetting and Oil/Water Emulsion Stability Applications. *Langmuir* **2021**, 37(35), 10560-10572.
6. Bergström, M.; Aratono, Synergistic effects in mixtures of two identically charged ionic surfactants with different critical micelle concentrations. M. *Soft Matter* **2011**, 7(19), 8870-8879.
7. Shortall, SM.; Marangoni, DG.; Wettig, SD. Mixing behaviour of Pluronics with gemini surfactant/plasmid DNA condensates: effect of Pluronic composition. *Phys. Chem. Chem. Phys.* **2020**, 22(45), 26121-26135.

8. Parmar, A.; Chavda, S.; Bahadur, P. Pluronic–cationic surfactant mixed micelles: Solubilization and release of the drug hydrochlorothiazide. *Colloids Surf. A Physicochem. Eng. Asp.* **2014**, 441, 389-397.
9. Vyas, B.; Pillai, A.; Bahadur, P. Influence of surfactant's polar head group charge on the self-assembly of three PEO–PPO–PEO triblock copolymers of widely varying hydrophobicity. *J. Mol. Liq.* **2020**, 316, 113858-113869.
10. McWilliams, A.; Reyes, C.; Liberman, L.; Ergülen, S.; Talmon, Y.; Pasquali, M.; Martí, A. Surfactant-assisted individualization and dispersion of boron nitride nanotubes. *Nanoscale Adv.* **2019**, 1(3), 1096-1103.
11. Patil, R.; Ray, D.; Aswal, V.; Bussy, C.; Bahadur, P.; Tiwari, S. Adsorption of P103 Nanoaggregates on Graphene Oxide Nanosheets: Role of Electrostatic Forces in Improving Nanosheet Dispersion. *Langmuir* **2021**, 37(2), 867-873.
12. Percival, S.; Mayer, D.; Kirsner, R.; Schultz, G.; Weir, D.; Roy, S.; Alavi, A.; Romanelli, M. Romanelli, Surfactants: Role in biofilm management and cellular behaviour. *Int Wound J.* **2019**, 16, 753–760.
13. Ghatak, P.; Mathew-Steiner, S. S.; Pandey, P.; Roy, S.; Sen, C. K. A surfactant polymer dressing potentiates antimicrobial efficacy in biofilm disruption. *Sci. Rep.* **2018**, 8:873, 1-9.
14. Mayer, D.; Armstrong, D.; Schultz, G.; Percival, S.; Malone, M.; Romanelli, M.; Keast, D.; Jeffery, S. Cell salvage in acute and chronic wounds: a potential treatment strategy. Experimental data and early clinical results. *J Wound Care*. **2018**, 27(9), 594-605.
15. Kaur, R.; Kumar, S.; Aswal, V.; Mahajan, R. Interactional and aggregation behavior of twin tail cationic surfactants with pluronic L64 in aqueous solution. *Colloid Polym. Sci.* **2012**, 290(2), 127-139.
16. Patel, D.; Ray, D.; Tiwari, S.; Kuperkar, K.; Aswal, V.; Bahadur, P. SDS triggered transformation of highly hydrophobic Pluronics® nanoaggregate into polymer-rich and surfactant-rich mixed micelles. *J. Mol. Liq.* **2022**, 345, 117812-117822.
17. Prameela, G.; Kumar, P.; Pan, A.; Aswal, V.; Subramanian, J.; Mandal, A.; Moulik, S. Physicochemical perspectives (aggregation, structure and dynamics) of interaction between pluronic (L31) and surfactant (SDS). *Phys. Chem. Chem. Phys.* **2015**, 17 (45), 30560-30569.
18. Kancharla, S.; Zoyhofski, A.; Bufalini, L.; Chatelais, F.; Alexandridis, P. Association between nonionic amphiphilic polymer and ionic surfactant in aqueous solutions: effect of polymer hydrophobicity and micellization. *Polymers* **2020**, 12 (8), 1831-1854.

19. Wang, P.; Pei, S.; Wang, M.; Yan, Y.; Sun, X.; Zhang, J. Coarse-grained molecular dynamics study on the self-assembly of Gemini surfactants: the effect of spacer length. *Phys. Chem. Chem. Phys.* **2017**, 19 (6), 4462-4468.
20. Jain, A.; Kishore N. Micellar properties of pluronics in combination with cationic surfactant and interaction with lysozyme: Thermodynamic evaluation. *J. Mol. Liq.* **2022**, 359, 119303-119318.
21. Vyas, B.; Pillai, S.; Tiwari, S.; Bahadur, P. Effects of head group and counter-ion variation in cationic surfactants on the microstructures of EO-PO block copolymer micelles. *Colloids Interface Sci. Commun.* **2019**, 33, 100216-100223.
22. Parmar, A.; Chavda, S.; Bahadur, P. Pluronic-cationic surfactant mixed micelles: Solubilization and release of the drug hydrochlorothiazide. Colloids and Surfaces A: Physicochem. *Eng. Aspects.* **2014**, 441, 389–397.
23. Poyraz, A.; Albayrak, C.; Dag, Ö. The effect of cationic surfactant and some organic/inorganic additives on the morphology of mesostructured silica templated by pluronics, *Microporous Mesoporous Mater*. **2008**, 115, 548–555.
24. Pérez-Sánchez, G.; Vicente, F.; Schaeffer, N.; Cardoso, I.; Ventura, S.; Jorge, M.; Coutinho, J. Rationalizing the phase behavior of triblock copolymers through experiments and molecular simulations. *J. Phys. Chem. C.* **2019**, 123(34), 21224-21236.
25. Pérez-Sánchez, G., Vicente, F.; Schaeffer, N.; Cardoso, I.; Ventura, S.; Jorge, M.; Coutinho, J. Unravelling the interactions between surface-active ionic liquids and triblock copolymers for the design of thermal responsive systems. *J. Phys. Chem. B.* **2020**, 124 (32), 7046-7058.
26. Pérez-Sánchez, G.; Schaeffer, N.; Lopes, M.; Pereira, F.; Coutinho, J. Using coarse-grained molecular dynamics to understand the effect of ionic liquids on the aggregation of Pluronic copolymer solutions. *Phys. Chem. Chem. Phys.* **2021**, 23 (10), 5824-5833.
27. Samanta, S.; Roccatano, D. Interaction of curcumin with PEO–PPO–PEO block copolymers: a molecular dynamics study. *J. Phys. Chem. B.* **2013**, 117 (11), 3250-3257.
28. Kacar, G. Molecular understanding of interactions, structure, and drug encapsulation efficiency of Pluronic micelles from dissipative particle dynamics simulations. *Colloid Polym. Sci.* **2019**, 297 (7), 1037-1051.
29. Yang, S.; Zhang, X.; Yuan, S. Mesoscopic simulation studies on micellar phases of Pluronic P103 solution. *J. Mol. Model.* **2008**, 14 (7), 607-620.
30. Patel, D.; Agarwal, S.; Ray, D.; Kuperkar, K.; Aswal, V.; Bahadur, P. An expedient in to the phase behaviour and scattering profile in PEO-PPO-PEO block copolymer mixed

systems in aqueous solution. *Colloids Surf. A Physicochem. Eng. Asp.* **2021**, 617, 126330-126340.

31. Patel, D.; Ray, D.; Kuperkar, K.; Aswal, V.; Bahadur, P. Parabens induced spherical micelle to polymersome transition in thermo-responsive amphiphilic linear and star-shaped EO-PO block copolymers. *J. Mol. Liq.* **2020**, 316, 113897-113908.
32. Pruitt J.; Husseini, G.; Rapoport, N.; Pitt, W. Stabilization of Pluronic P-105 Micelles with an Interpenetrating Network of N,N-Diethylacrylamide. *Macromolecules* **2000**, 33, 9306-9309
33. Kaur, R.; Kumar, S.; Aswal, V.; Mahajan, R. Influence of headgroup on the aggregation and interactional behavior of twin-tailed cationic surfactants with pluronics. *Langmuir* **2013**, 29 (38), 11821-11833.
34. Patel, D.; Patel, D.; Ray, D.; Kuperkar, K.; Aswal, V.; Bahadur, P. Single and mixed Pluronics® micelles with solubilized hydrophobic additives: Underscoring the aqueous solution demeanor and micellar transition. *J. Mol. Liq.* **2021**, 343, 117625-117637.
35. Páll, S.; Zhmurov, A.; Bauer, P.; Abraham, M.; Lundborg, M.; Gray, A.; Hess, B.; Lindahl, E. Heterogeneous parallelization and acceleration of molecular dynamics simulations in GROMACS. *J. Chem. Phys.* **2020**, 153 (13), 134110-134126.
36. Hockney, W.; Goel, S.; Eastwood, P. Eastwood, Quiet high-resolution computer models of a plasma. *J. Comput. Phys.* **1974**, 14 (2), 148-158.
37. Hess, B.; Bekker, H.; Berendsen, J.; Fraaije, J. LINCS: a linear constraint solver for molecular simulations. *J. Comput. Chem.* **1997**, 18 (12), 1463-1472.
38. Darden, T.; York, D.; Pedersen, L. Particle mesh Ewald: An N· log (N) method for Ewald sums in large systems. *Chem. Phys.* **1993**, 98 (12), 10089-10092.
39. Bussi, G.; Donadio, D.; Parrinello, M. Canonical sampling through velocity rescaling. *Chem. Phys.* **2007**, 126 (1), 014101-014109.
40. Parrinello, M.; Rahman, A. Polymorphic transitions in single crystals: A new molecular dynamics method. *J. Appl. Phys.* **1981**, 52 (12), 7182-7190.
41. Martínez, L.; Andrade, R.; Birgin, G.; Martínez, J. PACKMOL: a package for building initial configurations for molecular dynamics simulations. *J. Comput. Chem.* **2009**, 30 (13), 2157-2164.
42. Humphrey, W.; Dalke, A.; Schulten, K. VMD: visual molecular dynamics. *J. Mol. Graph.* **1996**, 14 (1), 33-38.
43. Jorge, L. Molecular dynamics simulation of self-assembly of n-Decyltrimethyl ammonium Bromide micelles. *Langmuir* **2008**, 24 (11),5714-5725.

44. Hoshen, J.; Kopelman, R. Percolation and cluster distribution. I. Cluster multiple labeling technique and critical concentration algorithm. *Phys. Rev. B Condens. Matter.* **1976**, 14 (8), 3438-3116.
45. Marrink, J.; Risselada, J.; Yefimov, S.; Tieleman, P.; Vries, D. The MARTINI force field: coarse grained model for biomolecular simulations. *J. Phys. Chem. B.* **2007**, 111 (27), 7812-7824.
46. Pérez-Sánchez, G.; Gomes, R.; Jorge, L. Modeling self-assembly of silica/ surfactant mesostructures in the templated synthesis of nanoporous solids. *Langmuir* **2013**, 29 (7), 2387-2396.
47. Sangwai, V.; Sureshkumar, R. Coarse-grained molecular dynamics simulations of the sphere to rod transition in surfactant micelles. *Langmuir* **2011**, 27 (11), 6628-6638.
48. Illa-Tuset, S.; Malaspina, C.; Faraudo, P. Coarse-grained molecular dynamics simulation of the interface behaviour and self-assembly of CTAB cationic surfactants. *Phys. Chem. Chem. Phys.* **2018**, 20 (41), 26422-26430.
49. Chien, C.; Pérez-Sánchez, G.; Gomes, R.; Cordeiro, D.; Jorge, M.; Auerbach, M.; Monson, C. Molecular simulations of the synthesis of periodic mesoporous silica phases at high surfactant concentrations. *J. Phys. Chem. C.* **2017**, 121 (8), 4564-4575.
50. Chavda, S.; Kuperkar, K.; Bahadur, P. Formation and growth of gemini surfactant (12-s-12) micelles as a modulate by spacers: a thermodynamic and small-angle neutron scattering (sans) study. *J. Chem. Eng. Data.* **2011**, 56 (5), 2647-2654.
51. Kulthe, S.; Inamdar, N.; Choudhari, Y.; Shirolikar, S.; Borde, L.; Mourya, C. Mixed micelle formation with hydrophobic and hydrophilic Pluronic block copolymers: implications for controlled and targeted drug delivery. *Colloids Surf. B: Biointerfaces.* **2011**, 88 (2), 691-696.
52. Sachin, K.; Karpe, A.; Singh, M.; Bhattarai, H. Study on surface properties of sodium dodecyl sulfate and dodecyltrimethylammonium bromide mixed surfactants and their interaction with dyes. *Heliyon* **2019**, 5 (4), 01510-01543.
53. Pisárčik, M.; Devínsky, F.; Pupák, C. Determination of micelle aggregation numbers of alkyltrimethylammonium bromide and sodium dodecyl sulfate surfactants using time-resolved fluorescence quenching. *Open Chem. J.* **2015**, 13 (1), 922-931.
54. Griffin, R.; Browning, L.; Truscott, L.; Clifton, A.; Webster, J.; Clarke, S. A comparison of didodecyldimethylammonium bromide adsorbed at mica/water and silica/water interfaces using neutron reflection. *J. Colloid Interface Sci.* **2016**, 478, 365-373.

55. Ono, Y.; Kawasaki, H.; Annaka, M.; Maeda, H. Effects of micelle-to-vesicle transitions on the degree of counterion binding. *J. Colloid Interface Sci.* **2005**, 287 (2), 685-693.
56. Feitosa, E.; Adati, D.; Alves, F. Thermal and phase behavior of didodecyldimethyl ammonium bromide aqueous dispersions. *Colloids Surf. A: Physicochem. Eng. Asp.* **2015**, 480, 253-259.
57. Caria, A.; Regev, O.; Khan, A. Surfactant-polymer interactions: phase diagram and fusion of vesicle in the didodecyldimethylammonium bromide–poly (ethylene oxide)–water system. *J. Colloid Interface Sci.* **1998**; 200 (1), 19-30.
58. Marques, F.; Regev, O.; Khan, A.; Miguel, M. Vesicle formation and general phase behavior in the catanionic mixture SDS-DDAB-water. The anionic-rich side *J. Phys. Chem. B.* **1998**, 102 (35), 6746-6758.
59. Deng, X.; Yang, Y.; Ma, Y.; Sun, X.; Zhou, G.; Wu, H..; Lu, G. Self-assembled structure of sulfonic gemini surfactant solution. *AIP Advances.* **2018**, 8 (7), 075003-075012.
60. Alargova, R.; Kochijashky, I.; Sierra, M.; Zana, R. Micelle aggregation numbers of surfactants in aqueous solutions: a comparison between the results from steady-state and time-resolved fluorescence quenching. *Langmuir* 14 (19) (1998) 5412-5418.
61. Dahanayake, R.; Dormidontova, E. E. Molecular Structure and Co-solvent Distribution in PPO–PEO and Pluronic Micelles. *Macromolecules* **2022,** doi.org/10.1021/acs.macromol.2c01206.
62. Lopez-Barro, C.; Chen, R.; Wagner, N.; Beltramo, P. Self-Assembly of Pluronic F127 Diacrylate in Ethylammonium Nitrate: Structure, Rheology, and Ionic Conductivity before and after Photo-Cross-Linking. *Macromolecules* **2016**, 49, 14, 5179–5189.
63. Kanoje, B.; Jangir, A.; Patel, D.; Ray, D.; Aswal, V.; Pal, H.; Parikh, J.; Kuperkar, K. Micellar transition (ellipsoidal to ULV) induced in aqueous Gemini surfactant (12-2-12) solution as a function of additive concentration and temperature using experimental and theoretical study, Colloids Surf. A: Physicochem. *Colloids Surf. A: Physicochem. Eng. Asp.* **2018**, 555, 227-236.
64. Kanoje, B.; Patel, D.; Kumara, V.; Sahoo, S.; Parikh, J.; Kuperkar, K. Unraveling the solubilization and cytotoxicity study of poorly water-soluble anti-inflammatory drug in aqueous Gemini surfactants solution with physicochemical characterization and simulation study. *Colloids Surf. B: Biointerfaces.* **2019**, 179, 437-444.
65. Patel, D.; Bhojani, K. A.; Ray, D.; Singh, K. D.; Bhattacharjee, S.; Seth, D.; Aswal, K. V.; Kuperkar, K.; Bahadure, P. Glucose-induced self-assembly and phase separation in

hydrophilic triblock copolymers and the governing mechanism. *Phys. Chem. Chem. Phys.* **2022**, 24, 21141–21156.

66. Patel, D.; Ray, D.; Aswal, K. V.; Kuperkar, K.; Bahadur, P. Micellar assembly leading to structural growth/ transition in normal and reverse Tetronics® in single and mixed solution environment. *Soft Matter.* **2022**, 18, 4543–4553.
67. Halacheva, S.; Rangelov, S.; Tsvetanov, C. Poly(glycidol)-Based Analogues to Pluronic Block Copolymers. Synthesis and Aqueous Solution Properties. *Macromolecules* **2006**, 39, 6845-6852.

# Supporting Information

## Rationalising design of Pluronics-surfactant mixed micelles through molecular simulations and experiments

Divya Patel[a], Germán Pérez-Sánchez[b], Miguel Jorge[c], Debes Ray[d,e], Vinod K. Aswal[d], Ketan Kuperkar[a,*], João A. P. Coutinho[b], Pratap Bahadur[f]

[a] *Department of Chemistry, Sardar Vallabhbhai National Institute of Technology (SVNIT), Ichchhanath, Surat-395 007, Gujarat, INDIA.*
[b]*CICECO – Aveiro Institute of Materials, Department of Chemistry, University of Aveiro, Aveiro, 3810-1933, PORTUGAL.*
[c]*Department of Chemical and Process Engineering, University of Strathclyde, 75 Montrose Street, Glassgow G1 1XJ, UNITED KINGDOM.*
[d]*Solid State Physics Division, Bhabha Atomic Research Centre (BARC), Trombay, Mumbai, 400 085, Maharashtra, INDIA.*
[e]*Biomacromolecular systems and processes, Institute of Biological Information Processing, Forschungszentrum Julich- 52428, GERMANY.*
[f]*Department of Chemistry, Veer Narmad South Gujarat University (VNSGU), Udhana-Magdalla road, Surat-395 007, Gujarat, INDIA.*

***Corresponding author:** E-mail: ketankuperkar@gmail.com

**Declaration of interest:** None

**Experimental:**

Small-angle neutron scattering experiments were performed at the SANS diffractometer at Guide Tube Laboratory, Dhruva Reactor, Bhabha Atomic Research Centre, Mumbai, India.[1] In SANS, one measures the coherent differential scattering cross-section ($d\Sigma/d\Omega$) per unit volume as a function of wave vector transfer $Q$ (= $4\pi \sin\vartheta/\lambda$, where $\lambda$ is the wavelength of the incident neutrons and $2\vartheta$ is the scattering angle). The mean wavelength of the monochromatized beam from neutron velocity selector is 5.2 Å with a spread of $\Delta\lambda/\lambda$ ~ 15%. The angular distribution of neutrons scattered by the sample is recorded using a number of 1 m long one-dimensional $He^3$ position-sensitive detectors (PSDs) in crossed-geometry. The instrument covers a $Q$-range of 0.017–0.35 $Å^{-1}$. The data have been analyzed by comparing the scattering from different models to the experimental data. The modelling of the SANS data is described in detail in the next section.

**Small-angle neutron scattering analysis**

The differential scattering cross-section per unit volume ($d\Sigma/d\Omega$) as measured for a system of monodisperse particles in a medium can be expressed as

$$\left(\frac{d\Sigma}{d\Omega}\right)(Q) = nV^2\left(\rho_p - \rho_s\right)^2 P(Q)S(Q) + B \qquad (1)$$

where $n$ denotes the number density of particles, $\rho_p$ and $\rho_s$ are, respectively, the scattering length densities of particle and solvent and $V$ is the volume of the particle.[2,3]

$P(Q)$ is the intraparticle structure factor and $S(Q)$ is the interparticle structure factor. $B$ is a constant term representing the incoherent background, which is mainly due to the hydrogen present in the sample.

Intraparticle structure factor $P(Q)$ is decided by the shape and size of the particle and is the square of single-particle form factor $F(Q)$ as determined by

$$P(Q) = \langle |F(Q)|^2 \rangle \qquad (2)$$

For a spherical particle of radius $R$, $F(Q)$ is given by[4]

$$F(Q) = 3\left[\frac{sin(QR) - QR\,cos(QR)}{(QR)^3}\right] \qquad (3)$$

For a prolate ellipsoidal particle with semi-major and semi-minor axes $a$ and $b$, respectively,

$$F(Q) = \int_0^1 F(Q,\mu)\ \mathrm{d}\mu \qquad (4)$$

where $$F(Q,\mu) = \frac{3(\sin x - x\cos x)}{x^3} \quad (5)$$

with $$x = Q\left[a^2\mu^2 + b^2(1-\mu^2)\right]^{1/2} \quad (6)$$

$\mu$ in the above equations refers to the cosine of the angle between the directions of $a$ and $Q$.

For a rod-like micelle of length $L = 2l$ and cross-sectional radius $R$,

$$P(Q) = \int_0^{\pi/2} \frac{\sin^2(Ql\ \cos\beta)}{Q^2l^2\ \cos^2\beta} \frac{4J_1^2(QR\ \sin\beta)}{Q^2R^2\ \sin^2\beta} \sin\beta\ d\beta \quad (7)$$

where $\beta$ is the angle between the axis of the rod and bisectrix. $J_1$ is the Bessel function of order unity.[5]

For a system of monodisperse unilamellar vesicles, $d\Sigma/d\Omega$ can be expressed as

$$\frac{d\Sigma}{d\Omega}(Q,R) = n(\rho_v - \rho_s)^2 \left[\frac{4}{3}\pi R^3 \frac{3J_1(QR)}{QR} - \frac{4}{3}\pi(R+t)^3 \frac{3J_1\left[Q(R+t)\right]}{Q(R+t)}\right]^2 \quad (8)$$

where $n$ denotes the number density of the vesicles, $\rho_v$ and $\rho_s$ are the scattering length densities of the vesicle bilayer and the solvent, respectively. $R$ is the radius of the vesicle and $t$ is the thickness of the bilayer.[6]

$J_1(x)$ is the first order Bessel function and is given by

$$J_1(x) = \frac{\sin x - x\cos x}{x^2} \quad (9)$$

$S(Q)$ depends on the correlation of the particles and hence interaction between the particles. In general, $S(Q)$ shows several maxima and minima of decreasing amplitude. The first peak in $S(Q)$ occurs at $Q_{max} \sim 2\pi/d$, where $d$ is the average distance between the particles. For an isotropic system, $S(Q)$ can be written as

$$S(Q) = 1 + 4\pi n \int [g(r) - 1] \frac{\sin Qr}{Qr} r^2 dr \quad (10)$$

where $g(r)$ is the radial distribution function. It is the probability of finding another particle at a distance $r$ from a reference particle centered at the origin.[7] The details of $g(r)$ depend on the interaction potential $U(r)$ between the particles. Thus, one has to have the knowledge of $U(r)$ for calculating $S(Q)$. This in turn implies that the measured $S(Q)$ can be used to obtain information about the interaction potential $U(r)$.

Here, $S(Q)$ has been calculated using the mean spherical approximation developed by Hayter and Penfold[4,8]. In this approximation, the particle (in this case, *micelle*) is treated as a

rigid equivalent sphere of diameter $d$ interacting with another micelle through a screened Coulomb potential $u(r)$ given by the relation:

$$u(r) = u_0 d \exp\left[-\kappa(r-d)\right]/r, \; r > d \tag{11}$$

Where $u_0$ is the potential at $r = d$ and the Debye-Huckle inverse screening length $\kappa$ is evaluated by using the expression

$$\kappa = \left(\frac{8\pi N_A e^2 I}{10^3 \varepsilon k_B T}\right)^{1/2} \tag{12}$$

Where $N_A$, $e$, $I$, $\varepsilon$, $k_B$ and $T$ denote Avogadro number, electronic charge, ionic strength of the micellar solution, dielectric constant of the solvent solution, Boltzmann constant, and absolute temperature, respectively.

The contact potential $u_0$ is given by

$$u_0 = \frac{Z^2 e^2}{\pi\varepsilon\,\varepsilon_0 \sigma (2+\kappa\sigma)^2} \tag{13}$$

where $\varepsilon_0$ is the permittivity of free space.

Fractional charge is calculated as $\alpha = Z/N_{agg}$, where $Z$ is the effective micellar charge.

The polydispersity in the size distribution of particles is incorporated using the following integration

$$\frac{d\Sigma}{d\Omega}(Q) = \int \frac{d\Sigma}{d\Omega}(Q,R) f(R) dR + B \tag{14}$$

where $f(R)$ is the size distribution of the vesicles and usually accounted by a log-normal distribution as given by

$$f(R) = \frac{1}{\sqrt{2\pi}R\sigma} exp\left[-\frac{1}{2\sigma^2}\left(ln\frac{R}{R_{med}}\right)^2\right] \tag{15}$$

where $R_{med}$ is the median value and $\sigma$ is the standard deviation (polydispersity) of the distribution.[7] The mean radius ($R_m$) is given by $R_m = R_{med} \exp(\sigma^2/2)$.

The data have been analyzed by comparing the scattering from different models to the experimental data and selecting the model that provided the best fit to the data. Throughout the data analysis, corrections were made for instrumental smearing, where the calculated scattering profiles were smeared by the appropriate resolution function to compare with the measured data[9]. The radius for spherical micelles, semi-major and semi-minor axes for ellipsoidal micelles, and cross-sectional radius and length for the rod-like micelles have been used as fitting parameters, and their analysed values are listed in the corresponding Tables. The

scattering length densities of the core, shell, solvent and background have also been fitted. The fitted parameters in the analysis were optimized using a nonlinear least-squares fitting program to the model scattering.

The aggregation number ($N_{agg}$) from SANS measurements has been calculated by using the following relationship:

$$N_{agg} = V_m/V_{PPO} \quad (16)$$

where $V_m$ is the micellar volume and is given by $V_m = 4\pi R^3/3$ with $R$ is the core radius of spherical micelles. For ellipsoidal micelles, $V_m = 4\pi ab^2/3$ where $a$ and $b$ are semi-major and semi-minor axes, respectively. $V_{PPO}$ is the molecular volume of the hydrophobic tail of the block copolymer and is calculated using the formula:

$$V_{PPO} = (n \times 96.3)\ Å^3 \quad (17)$$

where the volume of a single PO unit is 96.3 Å and n is the number of PO blocks in that particular block copolymer. In case of mixed micelles, it represents the hydrophobic part of the mixture and is given by:

$$V_h = V_h^1 + C_2/C_1 V_h^2 \quad (18)$$

where $V_h^1$ and $V_h^2$ are the molecular volumes of hydrophobic part of the micelle and additive, respectively. $C_1$ and $C_2$ are the concentrations of the micelle and additive, respectively.

**References**:


1. Aswal, V.; Goyal, P. Small-angle neutron scattering diffractometer at Dhruva reactor. *Curr. Sci.* **2000**, 7(79) 947-953.
2. Hayter J.; Penfold J. Determination of micelle structure and charge by neutron small-angle scattering. *Colloid Polym Sci.* **1983**, 261, 1022–1030.
3. Ray, D.; Aswal, V.; Kohlbrecher, J. Synthesis and Characterization of High Concentration Block Copolymer-Mediated Gold Nanoparticles. *Langmuir* **2011**, 27, 7, 4048–4056.
4. Hayter, J.; Penfold, J. Self-consistent structural and dynamic study of concentrated micelle solutions. J. Chem. Soc., Faraday Trans. **1981**, 1(77), 1851-1863.
5. Sikder, A.; Ray, D.; Aswal, V.; Ghosh, S. Hydrogen-Bonding-Regulated Supramolecular Nanostructures and Impact on Multivalent Binding.
6. Sikder, A.; Ray, D.; Aswal, V.; Ghosh, S. Hydrogen Bonding Regulated Supramolecular Nanostructures and Impact on Multivalent Binding. *Angew. Chem.* **2019**, 131(6), 1620-1625.

7. Ashcroft, N.; Lekner, J. Structure and Resistivity of Liquid Metals. *Phys. Rev.* **1966,** 145, 83 –90.
8. Pedersen J. Analysis of small-angle scattering data from colloids and polymer solutions: modeling and least-squares fitting. *Adv. Colloid Interface Sci.* **1997**, 70, 171-210.
9. Bevington, P. Data Reduction and Error Analysis for Physical Sciences. *McGraw-Hill, New York,* **1969**.

## METHODOLOGY

*Coarse-grained molecular model*

**Table S1.** Details of the CG-MD simulations carried out in this work.

| Simulation | Systems | L81 | Surfactant | W |
|---|---|---|---|---|
| run1 | L81/W | 50 | 0 | 190000 |
| run2 | DTAB/W | 0 | 240 | 90000 |
| run3 | DDAB/W | 0 | 500 | 370000 |
| run4 | 12-2-12/W | 0 | 500 | 530000 |
| run5 | L81/W | 50 | 0 | 62000 |
| run6 | L81/5 mM DTAB/W | 50 | 25 | 62000 |
| run7 | L81/1 0mM DTAB/W | 50 | 50 | 62000 |
| run8 | L81/30 mM DTAB/W | 50 | 152 | 62000 |
| run9 | L81/90 mM DTAB/W | 50 | 455 | 62000 |
| run10 | L81/5 mM 12-2-12/W | 50 | 25 | 62000 |
| run11 | L81/10 mM 12-2-12/W | 50 | 50 | 62000 |
| run12 | L81/30 mM 12-2-12/W | 50 | 152 | 62000 |
| run13 | L81/90 mM 12-2-12/W | 50 | 455 | 62000 |
| run14 | L81/5 mM DDAB/W | 50 | 25 | 62000 |
| run15 | L81/10 mM DDAB/W | 50 | 50 | 62000 |
| run16 | L81/30 mM DDAB/W | 50 | 152 | 62000 |
| run17 | L81/90 mM DDAB/W | 50 | 455 | 62000 |

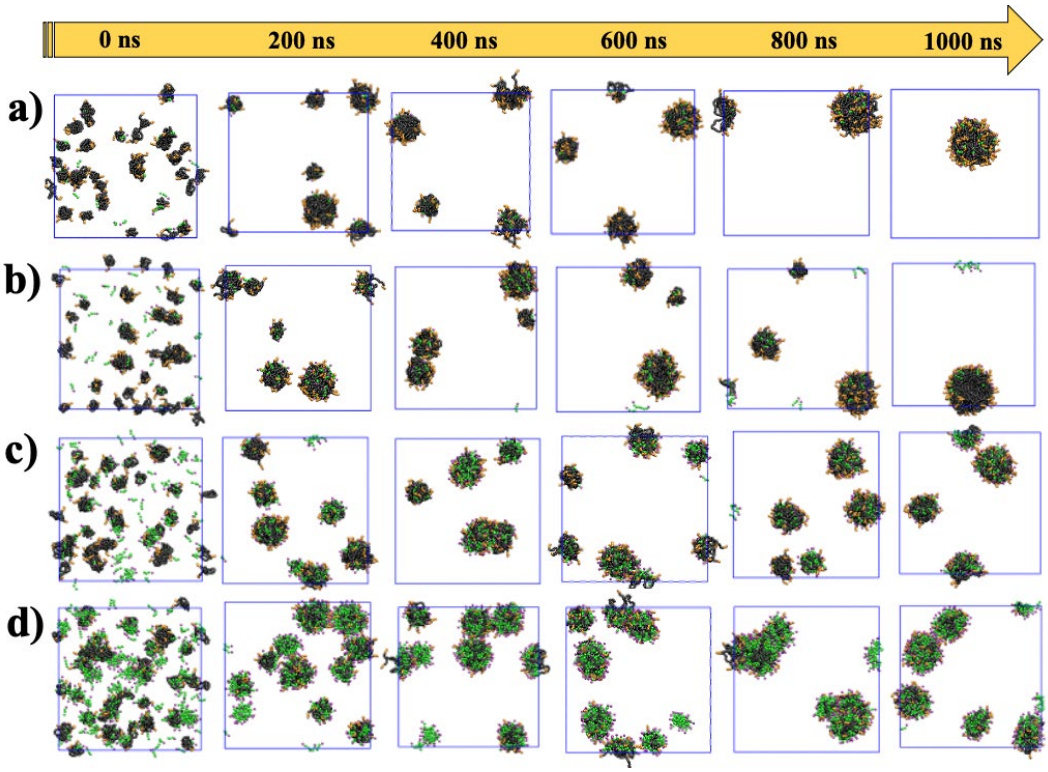


**Figure S1**. CG-MD simulation snapshots at different stages for the 3 %w/v L-81 aqueous solution mixed with a) 5mM, b) 10mM, c) 30mM and d) 90mM DTAB concentrations. The colour code is the same as in **Figure 11** and water molecules and bromide counterions were removed for clarity.

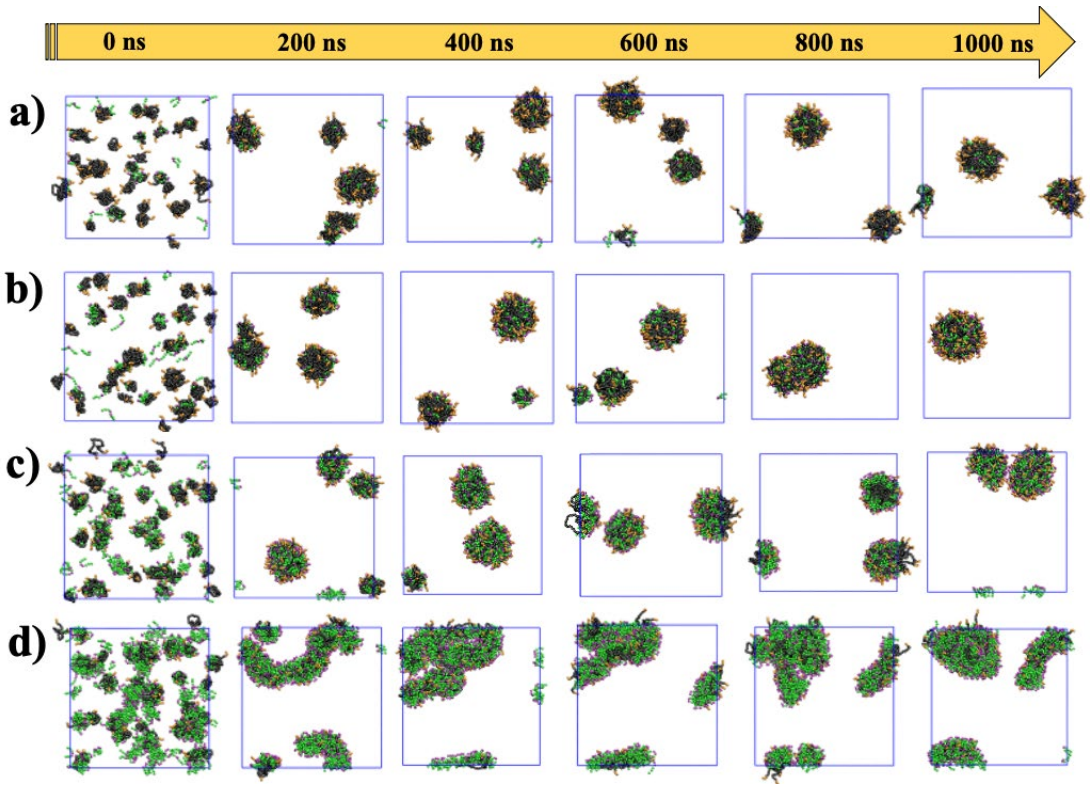


**Figure S2**. CG-MD simulation snapshots at different stages for the 3 %w/v L-81 aqueous solution mixed with a) 5mM, b) 10mM, c) 30mM and d) 90mM Gemini 12-2-12 concentrations. The colour code is the same as in **Figure 12** and water molecules and bromide counterions were removed for clarity.

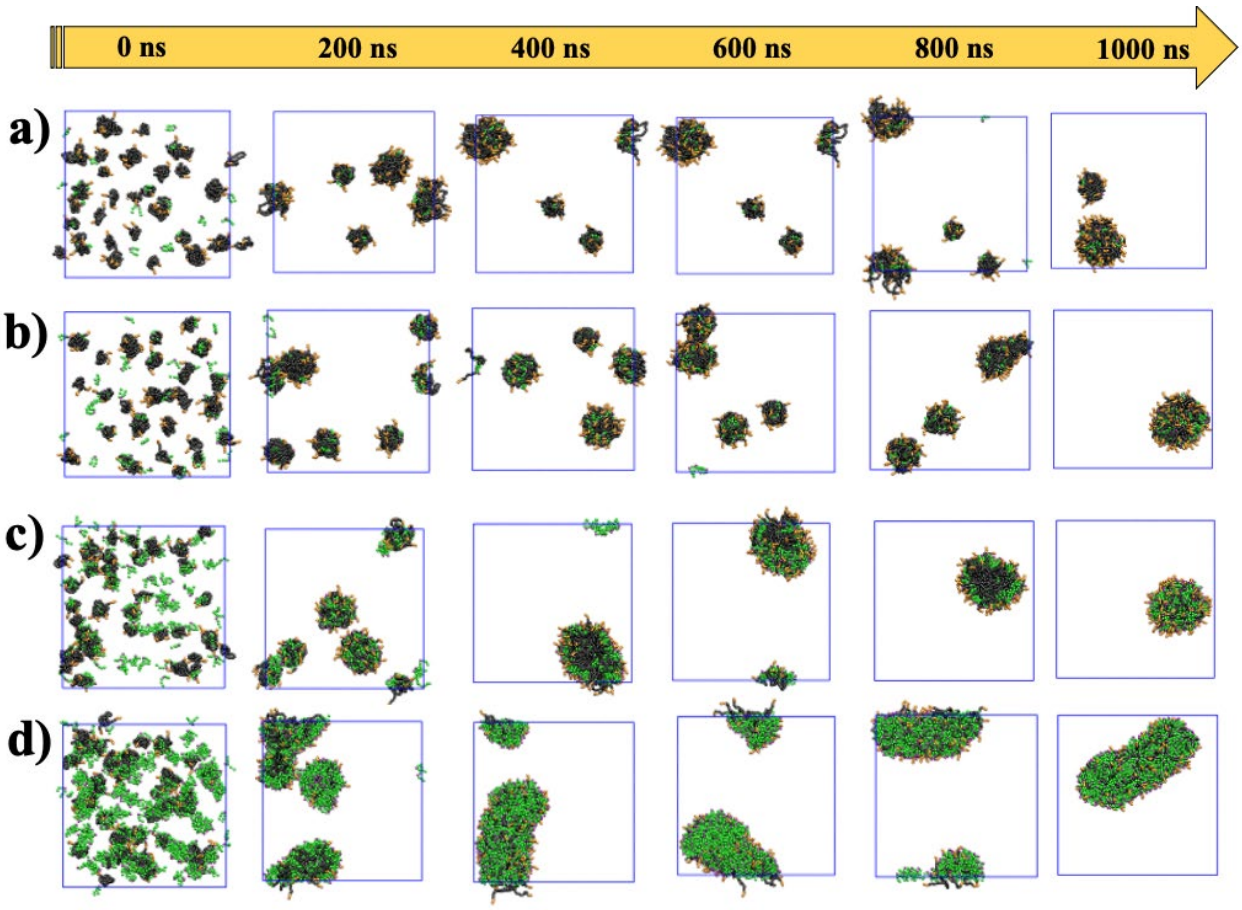


**Figure S3**. CG-MD simulation snapshots at different stages for the 3 %w/v L-81 aqueous solution mixed with a) 5mM, b) 10mM, c) 30mM and d) 90mM DDAB concentrations. The colour code is the same as in **Figure 13** and water molecules and bromide counterions were removed for clarity.